LAL/RT 94-07
July 1994



# Laboratoire de l'Accélérateur Linéaire

## CONTRIBUTIONS TO THE EPAC CONFERENCE

*4th European Particle Accelerator Conference*
*London, 27 June – 1 July, 1994*

U.E.R
de
l'Université Paris-Sud

Institut National
de Physique Nucléaire
et
de Physique des Particules

Bâtiment 200 - 91405 ORSAY Cedex

LAL/RT 94-07
July 1994

# CONTRIBUTIONS TO THE EPAC CONFERENCE

*4th European Particle Accelerator Conference*
*London, 27 June – 1 July, 1994*

LAL/RT/94-07
July 1994

# CONTRIBUTIONS TO THE EPAC CONFERENCE

**Review of Electron Guns**
C. Travier
*Invited paper at the 4th European Particle Accelerator Conference*
*London, 27 June – 1 July, 1994*

**First Operation of a Femtosecond Laser Driven Photo–injector**
C. Travier, M. Bernard, B. Leblond

**PRIAM/ANTIGONE : a 2D/3D Package for Accelerator Design**
G. Le Meur, F. Touze

**The TESLA Test Facility Linac Injector**
M. Bernard, J.C. Bourdon, R. Chehab, T. Garvey, B. Jacquemard, B. Mouton, M. Omeich, J. Rodier, P. Roudier, Y. Thiery

**On some RF Three–dimensional Simulation of Magnetically Coupled Cells**
M. Chanudet

**Dark Current under Low and High Electric Field**
G. Bienvenu, P. Brunet

**A Versatile TBA Lattice for a Tau–Charm Factory with and without Beam Monochromatization**
A. Faus–Golfe, J. Le Duff
*Contributed paper to the 4th European Particle Accelerator Conference*
*London, 27 June – 1 July, 1994*

# Review of Electron Guns

Christian Travier
Laboratoire de l'Accélérateur Linéaire
IN2P3-CNRS et Université de Paris-Sud
Bâtiment 200
F-91405 Orsay

*Abstract*

Most of present and future electron accelerators require bright sources. This review of electron guns therefore focuses on the brightest sources presently available, the photo-injectors. After briefly recalling their principle, the most advanced projects are reviewed. Photocathodes, lasers and photo-injector beam dynamics are then discussed.

## 1 INTRODUCTION

Numerous applications of electron linacs require high-brightness sources. These include high-energy linear colliders [1], short wavelength free electron lasers [2], wake-field accelerator experiments [3], new accelerator schemes test facilities [4], drive beam for two-beam accelerators [5], coherent radiation sources [6], radiochemistry [7], ...

The brightness being proportional to the peak current divided by the square of the normalized emittance, bright electron sources require intense beams (high charge and short pulse) and small emittances. Figure 1 shows the normalized brightness needed by linear colliders and FEL applications. It also shows the present state of the art of conventional injectors (DC gun + bunchers), thermionic RF guns and photo-injectors. This plot shows that a photo-injector allows on average two (respectively one) orders of magnitude improvement in brightness when compared to a conventional injector (respectively thermionic RF gun).

This potentiality of photo-injectors to produce bright beams has boosted their development. Since their invention 10 years ago at Los Alamos [8], the number of photo-injectors has rapidly increased and currently exceeds 30. Table 1 gives a summary of the main breakthroughs occured during the last ten years in the field of RF photo-injectors.

After a brief description of photo-injector principle, this review only focuses on the nine most advanced projects. Finally, general remarks concerning current trends of R&D in the field of photocathodes, lasers, and beam dynamics in a photo-injector are discussed.

## 2 PHOTO-INJECTOR PRINCIPLE

To increase the brightness of an electron source, it is necessary to increase its peak current while keeping a very small transverse emittance. This leads to use high electric field to reduce the influence of space charge forces. Since DC fields in a gun are limited to a few hundred kilovolts, it

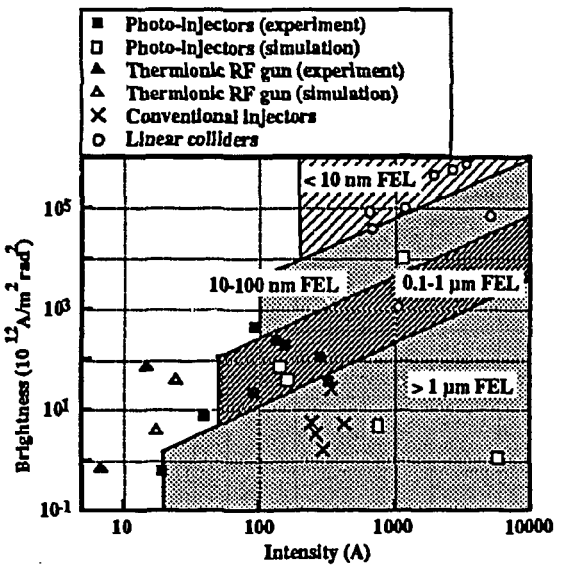


Figure 1: *Brightness required for FEL and linear colliders*

Table 1: Main breakthroughs in photo-injector history

| Date | Event | Ref. |
|---|---|---|
| 1985 | First photo-injector at Los Alamos | [8] |
| 1988 | First FEL driven by photo-injector at Stanford | [9] |
| 1988 | Emittance compensation theory by B. Carlsten | [10] |
| 1989 | First S-band photo-injector at Brookhaven | [11] |
| 1989 | Analytic theory of photo-injector beam dynamics by K.J. Kim | [12] |
| 1990 | First 144 MHz photo-injector at CEA | [13] |
| 1992 | First 433 MHz high duty cycle photo-injector at BOEING | [14] |
| 1992 | First photocathode in a superconducting RF cavity at Wuppertal | [15] |
| 1993 | UV FEL driven by photo-injector at Los Alamos | [16] |
| 1993 | First sub-picosecond laser driven photo-injector at LAL | [17] |
| 1994 | New analytic theory of photo-injector beam dynamics by L. Serafini | [18] |

is more appropriate to use RF fields to extract high peak current from a cathode. Following this idea has led G. Westenskow and J. Madey to design and operate in 1985, the first microwave gun consisting of a thermionic cathode located in an S-band RF cavity [19]. The necessity of high peak current led then to consider short pulses. The electronic grid switching of a conventional DC gun does not allow to produce pulses shorter than a few hundred picoseconds. To obtain shorter pulses, it is natural to think about optical switching. A short laser pulse illuminating a photocathode provides an almost ideal way to produce such short pulses. The combination of acceleration in an RF field and generation of electrons by short laser pulses hitting a photocathode make a quasi perfect bright injector. Today, lasers are able to produce very short pulses (down to less then 1 ps), photocathode can deliver high current densities (several thousands of $kA/cm^2$) and RF cavities can sustain electric field as high as 100 MV/m.

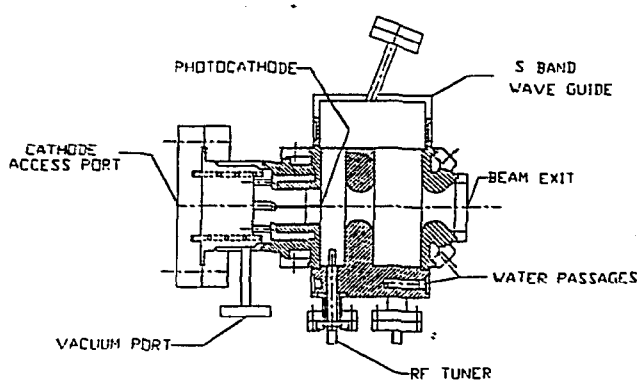


Figure 2: *BNL one and a half cell gun*

## 3 REVIEW OF ADVANCED PHOTO-INJECTORS

The most advanced photo-injector projects are reviewed below. The main features of each project are discussed. Table 2 summarizes the main parameters of each project. Except for ANL and MIT, the results correspond to experimental data and represent consistent sets of typical parameters. One should therefore be very careful while comparing these data since some of them (eg. emittance) are rather difficult to measure.

### *3.1 Los Alamos National Laboratory*

As already mentionned, the first photo-injector was designed and built at Los Alamos by J. Fraser and R. Sheffield [8]. After this first prototype, LANL has built APEX [20] and AFEL [21] photo-injectors. These devices are sophisticated guns made of several RF cells and using the emittance compensation scheme devised by B. Carlsten [10]. The APEX gun brightness was so high that it allowed the first UV FEL lasing on a linac [16]. AFEL gun is made of 6 cells and produces a very bright electron beam used to drive a very compact FEL. Present studies include a detailed understanding of emittance measurement techniques for these very bright beams.

### *3.2 Brookhaven National Laboratory*

The BNL gun design [22] shown in figure 2 is the most popular one, since it was already reproduced 10 times. The careful design of the cavity shape is intended to completely suppress higher spatial harmonics of the field, thus minimizing the non-linear emittance. The high gradient operation (up to 100 MV/m) allows to produce the very small emittance beams needed by the FEL and advanced accelerator physics experiments done at the Brookhaven ATF facility.

The most oustanding recent result is the convenient use of a magnesium cathode, that proved both to have a relatively good quantum efficiency ($5 \times 10^{-4}$) and be very robust (lifetime over 5000 hours).

This one and a half gun is now being replaced by a three and a half gun conjointely designed and fabricated by BNL and Grumman [23] and that can work at very high duty cycle (1%). A new laser system is also being assembled. Together with SLAC, UCLA, NRL, and LANL, BNL is now designing an inexpensive gun that would allow smaller laboratories or universities and smaller groups inside big laboratories to afford such a bright gun for any type of application.

### *3.3 CEA at Bruyères-le-Chatel*

At CEA, the photo-injector is made of one 144 MHz cavity and is used as the electron source for the infra-red high power FEL [13]. Recent emphasis has been put on improving the stability and reliability of the system. An amplitude feedback system is being developed to improve the laser stability.

### *3.4 CERN*

The CTF (CLIC Test Facility) was built at CERN to test some components of the CERN Linear Collider project [24] based on the concept of the two-beam accelerator. In order to generate the RF power at 30 GHz necessary to obtain the high accelerating gradient needed for the 30 GHz CLIC accelerating section, one accelerates a train of short intense electron bunches, that can produce RF power through electromagnetic interaction with a so-called tranfer structure. This train of intense short electron pulses is produced by a BNL type RF gun, using a $Cs_2Te$ photocathode. Recently a train of 24 pulses, 14 ps long and 1.6 nC each led to the production of 34 MW of 30 GHz RF power [25]. When running with a single pulse, a charge as high as 14 nC was extracted from this photo-injector. The $Cs_2Te$ photocathode presents a good combination of a very good quantum efficiency (2-5 %) and a good lifetime

Table 2: Parameters for the main photo-injectors

| Parameter | CEA | LANL | ANL | BNL | CERN | KEK | UCLA | LAL | MIT |
|---|---|---|---|---|---|---|---|---|---|
| Purpose | FEL | FEL | Wakefield accelerator | Advanced accelerator | Linear collider | Linear collider | FEL | Linear collider | High gradient |
| First operation | 1990 | 1992 | - | 1989 | 1990 | ? | ? | 1993 | - |
| Number of cavities | 1 | 11 | 1 | 1.5 | 1.5 | 1 | 1.5 | 2 | 1.5 |
| Frequency (MHz) | 144 | 1300 | 1300 | 2856 | 2998 | 2856 | 2856 | 2998 | 17136 |
| Cathode field (MV/m) | 28 | 20 | 90 | 70 | 100 | 40 | 83 | 50 | 250 |
| Cathode | $Cs_3K_2Sb$ | $Cs_2Te$ | Y | Cu | $Cs_2Te$ | CsSb | Cu | Cu | Cu |
| Quantum efficiency (%) | 3 | 5 | 0.05 | 0.001 | 2 | ? | ? | $5\times10^{-4}$ | 0.001 |
| Lifetime | 1 h | months | ? | $\infty$ | 70 h | ? | $\infty$ | $\infty$ | ? |
| Laser | YAG | YLF | Kr-F | YAG | YLF | YAG | YAG | Ti:sa | Ti:sa |
| Wavelength (nm) | 532 | 263 | 248 | 266 | 262 | 532 | 266 | 260 | 260 |
| Pulse length FWHM (ps) | 20-50 | 6 | 3 | 15 | 8 | 10 | 4 | 0.2 | 2 |
| Energy ($\mu$J) | 20 | 50 | 12000 | 300 | 1 | 100 | 300 | 250 | 200 |
| Spot size FWHM (mm) | 2-7 | 4 | 20 | 0.1-1 | 5 | ? | 0.6 | 4 | 1 |
| Energy (MeV) | 2 | 16 | 1.7 | 3 | 4 | 0.9 | 3.5 | 2.2 | 2.8 |
| Charge (nC) | 0.5-5 | 3 | 100 | 0.5 | 4 | 3.2 | 0.5 | 0.11 | 0.1-1 |
| Pulse length FWHM (ps) | 20-50 | 20 | 14 | 11 | 13 | ? | 5 | ? | 1.5 |
| Jitter (ps) | 3 | < 1 | <10 | <1 | <1 | ? | ? | ? | 2 |
| Normalized rms emittance ($\pi$ mm mrad) | 4@1nC | 5 | 130 | 4 | ? | ? | 10 | ? | 3@1nC |

(several months).

### 3.5 *KEK*

A 1 cell S-band RF gun was developped at KEK in view of JLC linear collider [26]. This gun is the only one working with relatively high accelerating gradient (40 MV/m) and using an alcaline cathode (CsSb). A special emphasis has therefore been put on the vacuum system design with the use of NEG pumping. Since linear colliders need polarized sources, KEK is working on the subject of polarized photocathodes [27].

### 3.6 *University of California at Los Angeles*

The UCLA RF gun is a modified BNL gun. It allows 70 degree laser illumination of the cathode that produces an enhancement of the quantum efficiency when compared to normal incidence. Extensive measurements and comparison to simulation were made and proved to be satisfactory [28].

### 3.7 *Laboratoire de l'Accélérateur Linéaire Orsay*

A two decoupled cell S-band RF gun was recently put into operation at LAL [17]. The cathode is illuminated by a Ti:sapphire laser that produces 0.2 ps pulses [29]. This project is the first sub-picoseconde laser driven photo-injector.

### 3.8 *Argonne National Laboratory*

In order to do wakefield accelerator experiments, it is necessary to generate a very intense and short electron bunch [3]. At ANL, a photo-injector designed to produce 100 nC pulses is being commissioned. To maintain a pulse as short as possible in spite of the enormous space charge forces, a concave shape of the laser wavefront is created [30]. To probe the wakefield excited by this intense pulse, a second pulse is generated by a 7 cell photo-injector. An alternative design for this witness beam gun is a dielectric loaded cavity that allows to produce a perfectly linear acccelerating field [31].

### 3.9 *Massachussets Institute of Technology*

The MIT photo-injector is a one and a half BNL type gun scaled at 17 GHz [32]. The use of such a high frequency makes possible very high accelerating gradient. 250 MV/m is envisaged for this gun now under commissioning.

## 4 PHOTOCATHODES

A good photocathode for photo-injector operation should ideally have a high quantum efficiency (> 1 %) at infrared or visible wavelength, have a long lifetime (> several months) under moderate vacuum conditions, and be easy to prepare and install in the gun cavity. Such a perfect cathode does not exist yet, but progress were made recently, especially with $Cs_2Te$ and Mg cathodes. Table 3 shows the most commonly used photocathodes and a summary of their main advantages and drawbacks.

The only photocathode presently available to generate polarized electron is GaAs. However this cathode that is extensively studied [33] has never been used in an RF gun so far [34].

The choice of the photocathode to be used depends on the type of applications. It depends of course on the charge required from a single pulse, but also on the pulse format via the existence or not of a suitable laser. The typical cases are the following:

Table 3: Main photocathodes used in photo-injectors

| Cathode | Advantage | Drawback |
|---|---|---|
| $Cs_3Sb$, $CsK_2Sb$, ... | high quantum efficiency<br>0.5 $\mu$m laser | difficult to prepare<br>short lifetime<br>do not sustain high field<br>expensive preparation chamber and transfer system<br>need good vacuum |
| $Cs_2Te$ | high quantum efficiency<br>long lifetime<br><br>sustain high field | need UV laser<br>expensive preparation chamber and transfer system<br>response to train? |
| Cu, Y, Mg | no preparation chamber<br>long lifetime<br>fast response<br>sustain very high field<br>*sustain bad vacuum* | low quantum efficiency (except Mg)<br>need UV laser |
| $LaB_6$, WCaOBaO | no preparation chamber<br>long lifetime | low quantum efficiency<br>need UV laser<br>need to be heated prior to operation |

- if a single pulse of charge below 5 nC, is required, a Mg photocathode is probably the best choice.
- if train a pulses of charge less than a few nC are required, then one should probably go to $Cs_2Te$.
- for very high repetition rate or very high duty cycle and high charge, it is probably difficult to avoid $CsK_2Sb$.

## 5 LASERS

One of the key components of a photo-injector system is the laser. Amplitude, phase and position stability of the electron beam depend almost completely on the laser performances. A laser is typically made of an oscillator that generates a continuous train of pulses of small energy (few nJ). This oscillator is synchronized via an appropriate electronic system to a sub-harmonic of the RF frequency (typically 100 MHz). One single pulse or a train of a few hundred pulses is then selected through a Pockells cell and is then amplified. There exist several types of amplifiers (single pass, multiple pass, regenerative, ...) and according to the energy desired, it might be necesssary to have several amplifier stages. When the oscillator pulse is very short, one has to extend the pulse temporally before amplification to avoid damage of the amplifier cavity components. The pulse is then compressed back to its original duration. This technique is called the chirped pulse amplification. The oscillators used so far for photo-injector applications produce infra-red light. To obtain usable light for the photo-cathode, it is therefore necessary to generate higher harmonics. This is done by using non-linear crystals, with a typical efficiency of 10-15% from the fundamental to the third harmonic.

Nd:YAG and Nd:YLF (eg. [35]) are the most commonly used systems in existing photo-injectors. They typically produce pulses of 6-15 ps, with up to 300 $\mu$J of energy in a single pulse. More recently the advent of Ti:sapphire has open a way down towards the very short pulses (eg. [29]).

The recent progress of diode pumping made possible the design of very compact, stable, reliable and relatively cheap Nd:YLF oscillators. More work has yet to be done to improve the performances of amplifiers and harmonic generation in terms of output energy, amplitude stability and beam quality.

Sophisticated feedback and feedforward loops are now being envisaged to improve the different types of stability. Temporal and spatial filters allow in principle to produce any longitudinal and transverse profile, at the expense of energy. These features are interesting to do experimental tests of theoritical schemes developped to reduce the transverse emittance.

The R&D on short pulse lasers relevant foWashington, May 17-20,r photo-injector application is described in detail in references [36, 37].

## 6 BEAM DYNAMICS

RF gun beam dynamics was worked out in an analytical manner by K.J. Kim [12]. This simple model provides the gun designer with handy formulas for the different gun parameters, and are especially useful to understand the scaling of these parameters with such variables as the bunch length, the spot size on cathode, the peak accelerating field or the bunch charge. An improved model giving more accurate results, especially for the transverse bunch dimension was recently derived by L. Serafini [18].

Most of the theoritical work done on RF gun beam dynamics concerns the possibility to obtain smaller emittances, either by compensating the correlated emittance generated mainly in the first cell, or by removing the causes of extra emittance growth. Most of these techniques are

reviewed in reference [38]. Not all of them were experimentally proven or even tested. The most successfull one is the compensation of the correlated linear space charge induced emittance by the use of a magnetic focusing solenoid, due to B. Carlsten [10]. This technique experimentally proven at Los Alamos allows a ten fold reduction of the emittance. Once thought unapplicable at high frequencies and high gradient, it will soon be implemented at BNL [39].

Besides emittance compensation schemes, recent ideas being studied include travelling wave RF gun [40] and asymetric guns for linear colliders [41].

## 7 CONCLUSION

Ten years after its invention, the photo-injector has reached the point where it is used daily at users facility (cf BNL), and where it opened the way to new results such as UV FEL and the generation of 30 GHz power. When the remaining problems mainly concerning the laser stability and reliability will be solved, and that should not take too long, the photo-injector will be ready to replace the conventional DC gun + buncher injector for any kind of application. It will then be possible to have a 100 times brighter injector, 10 times more compact, and probably for less than half the price.

## 8 ACKNOWLEDGEMENTS

The data for the different projects were kindly provided by I. Ben Zvi, S.C. Chen, S, Joly, I. Madsen, R. Sheffield, P. Schessow, M. Yoshioka. Discussions with P. Georges were appreciated when writing the laser section. This paper benefited from the discussions of the source working group during the last Advanced Accelerator Concepts Workshop at Lake Geneva, WI.

## 9 REFERENCES

[1] R. Siemann, Proc. of the 1993 Particle Accelerator Conference, Washington, May 17-20, 1993.

[2] R. Sheffield, Proc. of the 1991 Particle Accelerator Conference, San Francisco, CA, May 6-9, 1991, pp. 1110-1114.

[3] P. Schoessow et al., Proc. European Particle Accelerator Conference, Nice, June 12-16, 1990, pp. 606-608.

[4] I. Ben-Zvi, AIP Proc. 279, 1993, pp. 591-607.

[5] K. Hübner, Proc. International Conference on High Energy Accelerators, Hamburg, July 20-24, 1992.

[6] P. Kung et al., SLAC-PUB-6426, 1994.

[7] J. Amblard, J. Belloni, "Projet Elyse", Univ. Orsay, Juin 1992.

[8] J. Fraser, R. Sheffield, Nucl. Instr. & Meth. A250 (1986), pp. 71-76.

[9] M. Curtin et al., Nucl. Instr. & Meth. A296 (1991), pp. 127-133.

[10] B. Carlsten, Nucl. Instr. & Meth. A285 (1989), pp. 313-319.

[11] K. Batchelor et al., Proc. European Particle Accelerator Conference, Nice, June 12-16, 1990, pp. 541-543.

[12] K.J. Kim, Nucl. Instr. & Meth. A275 (1989), pp. 201-218.

[13] S. Joly et al., Proc. European Particle Accelerator Conference, Nice, June 12-16, 1990, pp. 140-142.

[14] D.H. Dowell et al., Proc. Particle Accelerator Conference, Washington, May 17-20, 1993.

[15] A. Michalke et al., Proc. European Particle Accelerator Conference, Berlin, March 24-28, 1992, pp. 1014-1016.

[16] P.G. O'Shea et al., Physical Review Letters, Vol. 71, No 22, 1993.

[17] C. Travier et al., these proceedings.

[18] L. Serafini, Proc. Advanced Accelerator Concepts Workshop, Lake Geneva, June 13-18, 1994.

[19] G. Westenskow, J. Madey, Laser and Particle Beams (1984), Vol. 2, Part 2, pp. 223-225.

[20] D. Feldman et al., Proc. Linear Accelerator Conference, Ottawa, August 24-28, 1992.

[21] R. Sheffield et al., Proc. of the 1993 FEL Conference.

[22] K. McDonald, DOE/ER/3072-43, Princeton University, 1988.

[23] I. Lehrman et al., Nucl. Instr. & Meth. A318 (1992).

[24] Y. Baconnier et al., Proc. Linear Accelerator Conference, Ottawa, August 24-28, 1992, pp. 329-331.

[25] R. Bossart et al., these proceedings.

[26] M. Yoshioka et al., Proc. of the International Conference on High Energy Accelerators, Hamburg, July 20-24, 1992.

[27] T. Omori et al., Proc. of the International Conference on High Energy Accelerators, Hamburg, July 20-24, 1992.

[28] S. Hartman et al., Nucl. Instr. & Meth. A340 (1994), pp. 219-230.

[29] P. Georges et al., Proc. Particle Accelerator Conference, Washington, May 17-20, 1993, pp. 3053-3054.

[30] W. Gai et al., Proc. Particle Accelerator Conference, Washington, May 17-20, 1993, pp. 3050-3052.

[31] J. Power et al., Proc. Particle Accelerator Conference, Washington, May 17-20, 1993, pp. 3061-3062.

[32] S.C. Chen et al., Proc. Particle Accelerator Conference, Washington, May 17-20, 1993, pp. 2575-2577.

[33] Proc. of the Workshop on Photocathodes for Polarized Electron Sources for Accelerators, Stanford, September 8-10, 1993, SLAC-432.

[34] J. Clendenin et al., Nucl. Instr. & Meth. A340 (1994), pp. 133-138.

[35] J. Early et al., Nucl. Instr. & Meth. A318 (1992), pp. 381-388.

[36] K. Geissler, Nucl. Instr. & Meth. A340 (1994), pp. 52-73.

[37] Proc. Workshop Lasers for RF Guns, Anaheim, May 14-15, 1994.

[38] L. Serafini, Nucl. Instr. & Meth. A340 (1994), pp. 40-51.

[39] J.C. Gallardo, H. Kirk, Proc. Particle Accelerator Conference, Washington, May 17-20, 1993.

[40] J. Gao, Proc. European Particle Accelerator Conference, Berlin, March 24-28, 1992, pp. 584-586.

[41] J. Rosenzweig et al., Proc. Particle Accelerator Conference, Washington, May 17-20, 1993, pp. 3021-3023.

# First Operation of a Femtosecond Laser Driven Photo-injector

C. Travier, M. Bernard, B. Leblond
Laboratoire de l'Accélérateur Linéaire
IN2P3-CNRS et Université de Paris-Sud
Bâtiment 200
F-91405 Orsay
P. Georges, G. Roger, P. Thomas
Institut d'Optique Théorique et Appliquée
Université de Paris-Sud
Bâtiment 501
F-91405 Orsay

*Abstract*

CANDELA photo-injector is a two cell S-band photo-injector. The copper cathode is illuminated by a 200 fs Ti:sapphire laser. This paper presents the preliminary experimental results. Measurements of the beam charge as a function of the laser/RF phase, the laser pulse energy, and the accelerating field are presented.

## 1 INTRODUCTION

CANDELA photo-injector is a two decoupled cell 3 GHz RF gun. Its design is described in references [1, 2, 3]. The Ti:sapphire laser system designed by the "Institut d'Optique Théorique et Appliquée" at Orsay is presented in reference [4]. The RF conditionning of the gun and the dark current measurements are reported in reference [5]. This present paper concentrates on the first experimental results about photo electrons. The preliminary experiments reported were done during the fourth trimester of 1993. Since the laser illuminating the cathode has a pulse length of 200 fs, and since all other photo-injectors in the world have lasers with pulse length longer then 1 ps [6], this experiment can be considered as the first photo-injector driven by a "femtosecond" laser.

The only measurable parameter at the time of the experiments was the pulse charge. Therefore the results presented here show the variation of the charge with the following parameters: laser/RF phase, laser energy, and accelerating field.

## 2 EXPERIMENTAL SETUP

The gun described in reference [3], is powered by an old THOMSON TV2013 that can deliver a maximum measured peak power of 2.6 MW. This power is shared between the two cells in a way that the peak accelerating field is equal in the two cells. Its value at full power is 65 MV/m. In these preliminary experiments, the RF phase between the two cells was kept fixed.

Right at the gun exit, a wall current monitor (WCM) allows to measure the peak current and the position of the beam. The beam then goes into a coaxial Faraday cup having a 3 GHz bandwidth. The signal from the WCM and the Faraday cup are recorded on a TEKTRONIX TDS520 oscilloscope. Figure 1 shows a schematic of the experimental arrangement.

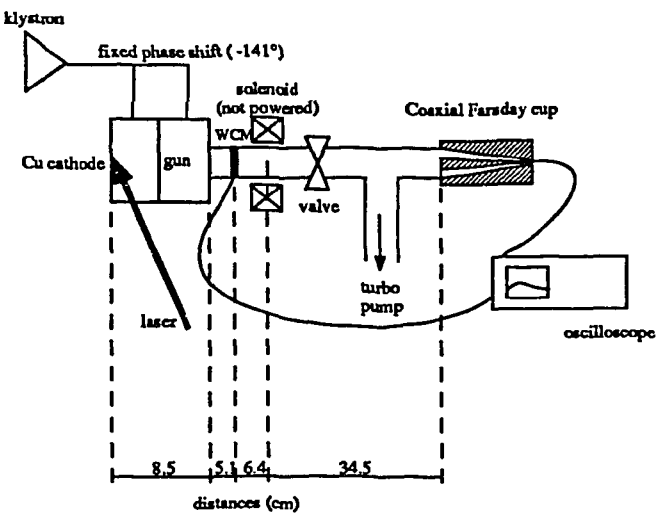


Figure 1: *Experimental setup*

The laser is a Ti:sapphire laser described in reference [4]. It produces one single pulse (at 12.5 Hz), 200 fs long with an energy of 225 $\mu$J at 260 nm. The optical path between the laser room and the gun cathode (around 25 m long) includes several lenses that were not covered by an anti-reflection coating at the time of the experiment. The overall efficiency of the light transport was therefore as low as 50%. The laser light is injected into the gun via one of the two 54°30' entry port. The laser is focused onto the cathode and its size is roughly estimated to be 5 mm.

The laser is synchronized to the RF frequency via an

electronic feedback loop that is driving a piezo-electric transducer that adjusts the laser oscillator cavity length. Due to problems with the mounting of the cavity mirror on the piezo transducer, the overall bandwidth of the feedback loop was not large enough to ensure a small jitter between the laser and the RF wave. This jitter was typically 40 ps rms. This fact made the measurements very uneasy, since this jitter led to large amplitude fluctuation of the signal.

# 3 EXPERIMENTAL RESULTS

## 3.1 *Typical signal*

Figure 2 shows a typical signal of the photo-current pulse seen by the Faraday cup. The width of the signal is due to the long cable that transports it to the control room.

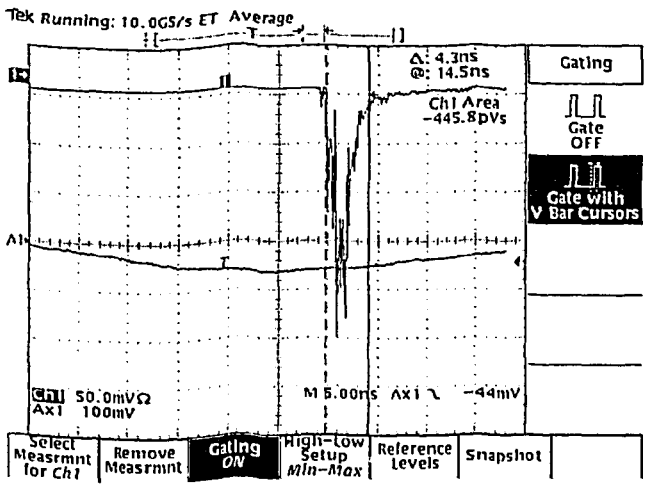


Figure 2: *Typical Faraday cup signal from a photo-current pulse (top trace)*

## 3.2 *Charge vs. relative laser/RF phase*

Only a certain span of the relative phase between the laser and the RF wave allows acceleration of the electrons emitted by the photocathode. Figure 3 presents the extracted charge as a function of the laser/RF phase, showing that the possible phases only span over 120 degrees. The triangular shape of this curve is due to a rather large spot size when compared to the beam aperture of the cavity. If the phase is not optimized, the outer electrons are easily scraped by the cavity aperture. This explanation is supported by a simulation made with the PIC code PRIAM [7]. If the laser spot size is made smaller, the shape of the curve "current vs. phase" looks like a trapezoid.

## 3.3 *Charge vs. laser energy*

Figure 4 shows the charge as a function of the laser energy on the cathode, measured both by the Faraday cup

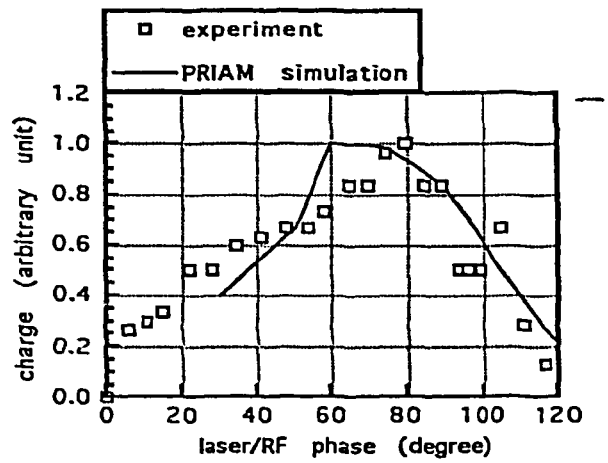


Figure 3: *Charge vs. relative phase between laser and RF*

and the WCM. The slight discrepancy between the two measurements is due to the fact that the WCM signal is recorded on one of the four outputs, while beam was not well centered. From the slope of the Faraday cup curve, it is possible to calculate the effective quantum efficiency of the cathode. Its value is $5 \times 10^{-6}$, which is already rather high for copper. It should be noted here that this set of measurements was made for a rather low accelerating field of 55 MV/m.

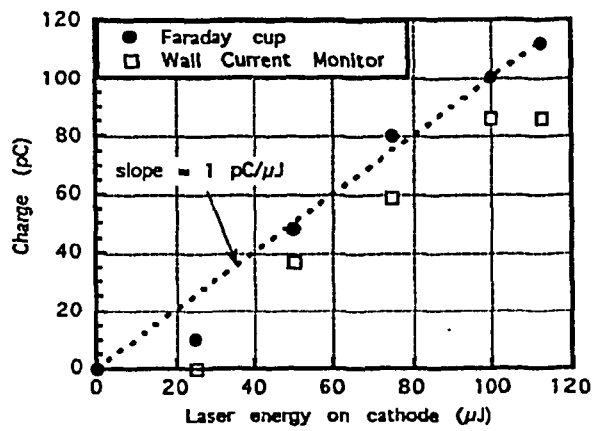


Figure 4: *Charge vs. laser energy*

## 3.4 *Charge vs. accelerating gradient*

Figure 5 shows the variation of the charge with the accelerating gradient. The fit shown on the figure represents Schottky law. According to this law, the emitted current

is expressed by:

$$J = aI(h\nu - \phi + \sqrt{\beta E})^2 \quad (1)$$

where $a$ is a constant, $I$ is the laser energy, $h\nu$ the photon energy, $\phi$ the work function of the cathode materiel, $\beta$ the field enhancement factor and $E$ the electric field on cathode. Similar behaviour was also measured at Brookhaven [8].

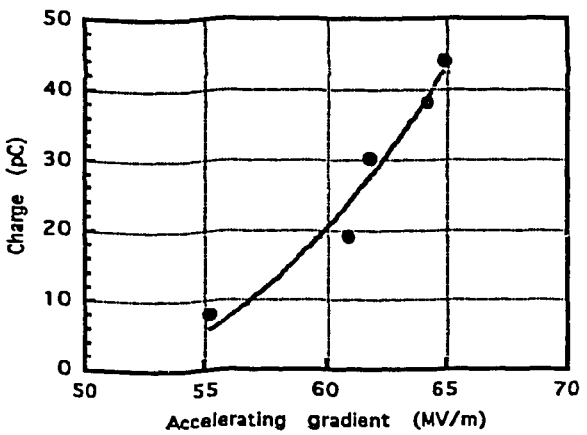


Figure 5: *Charge vs. accelerating gradient*

## 4 CONCLUSION

The first photo-electrons produced by a femtosecond laser driven RF gun were measured. A total charge of 0.11 nC was extracted under moderate accelerating field. A separate measurement has shown that due to Schottky effect, going to higher field would increase by a rather large factor the emitted charge. As we install the beam transport line and the various diagnostics, other beam characteristics will be measured.

## 5 ACKNOWLEDGEMENTS

These results would not have been possible without the involvement of a large number of people.

## 6 REFERENCES

[1] C. Travier, J. Gao, Proc. European Particle Accelerator Conference, Nice, June 12-16, 1990, pp. 706-708.

[2] C. Travier, J. Gao, H. Liu, Proc. Linear Accelerator Conference, Albuquerque, September 10-14, 1990, pp. 602-604.

[3] J. Gao et al., Proc. European Particle Accelerator Conference, Berlin, March 24-28, 1992, pp. 1020-1022.

[4] P. Georges et al., Proc. Particle Accelerator Conference, Washington, May 17-20, 1993, pp. 3053-3054.

[5] C. Travier et al., Nucl. Instr. & Meth. B89 (1994), pp. 27-32.

[6] C. Travier, Particle Accelerators, 1991, Vol. 36, pp. 33-74.

[7] G. Le Meur, F. Touze, these proceedings.

[8] X.J. Wang et al., Measurements on Photoelectrons from a Magnesium Cathode in a Microwave Electron Gun, submitted to J. Appl. Phys., 1994.

# PRIAM/ANTIGONE : a 2D/3D Package for Accelerator Design

Guy Le Meur, François Touze
Laboratoire de l'Accélérateur Linéaire
IN2P3-CNRS et Université Paris-Sud
91405 Orsay Cedex France

*Abstract*

The status of the finite element package PRIAM/ANTIGONE, developed at LAL for electromagnetic engineering, is presented. A short review of the available capabilities of the package is given.

## 1 INTRODUCTION

The design of accelerators and detectors needs computing tools for solving the Maxwell's equations in two as well as in three dimensions. There exist for a long time different programs treating electromagnetic problems, which are based on finite difference methods. The finite difference methods are popular, mainly because they seem to be staightforward to implement. However they present some drawbacks as, for instance, the necessity of special treatments on the boundaries or the difficulty of moduling the density of the mesh of the computed structure.
Finite element methods do not present these drawbacks ; that is why they are more and more used in the electromagnetic domain. An other advantage of using these methods is the possibility of coupling electromagnetic calculations with mechanical, thermal or other calculations, where f.e.m. are widely implemented for a long time.
We present here the status of a package developed at LAL [1], PRIAM for 2D case and ANTIGONE for 3D, using Raviart-Thomas [2] and Nedelec [3] finite elements based on the properties of the operators *div* and *curl* involved in the Maxwell's equations and related to the well-known physical laws : Gauss's, Ampère's, Faraday's. Applications of the code are described by other authors in this conference [4].

## 2 THE FOUR VECTORS DESCRIBING THE ELECTROMAGNETIC FIELD

The electromagnetic field is characterized by four vector fields : $\vec{E}, \vec{D}, \vec{B}, \vec{H}$ satisfying the four Maxwell's equations :

$$\frac{\partial \vec{D}}{\partial t} + curl\, \vec{H} = \vec{j} \qquad (1)$$

$$\frac{\partial \vec{B}}{\partial t} + curl\, \vec{E} = 0 \qquad (2)$$

$$div\, \vec{D} = \rho \qquad (3)$$

$$div\, \vec{B} = 0 \qquad (4)$$

together with the constitutive relations :

$$\vec{D} = \varepsilon \vec{E}$$
$$\vec{B} = \mu \vec{H} \qquad (5)$$

$\rho$ and $\vec{j}$ are respectively the charge and current density, $\varepsilon$ and $\mu$ are permittivity and permeability of the medium.

When solving these equations on a bounded domain one has to take into account boundary conditions and, in the case of evolutive problems, initial conditions.
In applying numerical formulations one usually takes care of the continuity of the physical quantities as potential or fields. This point is important in presence of different media in the structure : the right continuities have to be ensured on the interfaces. The problem may be not trivial, if the choice of the numerical method is not adapted. Concerning the Maxwell's equations it is worth noting that only normal components of $\vec{D}$ and $\vec{B}$ and tangential component of $\vec{E}$ and $\vec{H}$ are continuous on interfaces between different media. In a similar manner the boundary conditions are of two types : perfectly conducting walls where tangential components of $\vec{E}$ and $\vec{H}$ vanish and symmetry boundaries where normal components of $\vec{D}$ and $\vec{B}$ vanish.

## 3 A MADE -TO-MEASURE FINITE ELEMENT FORMULATION

Take, for example, the electrostatic problem. The principle of a "classical" f.e.m. would be to search the potential under the form of a linear combination of well chosen basis functions (or interpolation functions) $w_i(x,y,z)$ :

$$V(x,y,z) = \sum_{i=1}^{N} V_i\, w_i(x,y,z) \qquad (6)$$

the unknowns of the problem, $V_i$ , beeing the values of potential on "nodes" of a mesh which can be irregular. N is the total number of these nodes. The formulation is consistent if the $w$'s satisfy the following relations (if $x_j, y_j, z_j$ are the coordinates of the node number j) :

$$w_i(x_j, y_j, z_j) = \delta_{ij}$$

(Kronecker's symbol)

The electrostatic problem may be solved, for example, by putting the above expression for V in Euler's equations of the electrostatic energy minimization problem (variational formulation) leading to a linear system for the $V_i$ 's. If, for instance, the computational domain is meshed with tetrahedras (what we will assume from now on), the linear approximation consists of taking the vertices as nodes and the barycentric coordinates as basis fonctions. By this method we

get continuous potentials. The electric field derivated from this potential is not continuous, nor its tangential component on interfaces. In the following, this finite element will be called "P1".

There exist a little bit more sophisticated, so called "mixed" finite elements. Through this formulation, the calculated quantity is not only the potential but both $\vec{D}$ and V. $\vec{D}$ is searched under the form :

$$\vec{D}(x,y,z) = \sum_{i=1}^{N_d} \Phi_i \vec{N}_i(x,y,z) \qquad (7)$$

The unknowns $\Phi_i$ beeing now fluxes of $\vec{D}$ through the faces of the tetrahedras (in the case of linear approximation). Consequently the basis functions have to satisfy :

$$\iint_{F_j} \vec{N}_i . \vec{n}_j dS = \delta_{ij} \qquad (8)$$

This surface integral is taken over the face number j, $\vec{n}_j$ is the unit vector normal to that face, outgoing from the tetrahedron to which the basis vector function is related. For consistency reasons V is supposed to be constant in each tetrahedron.

These expressions are put, as before, in Euler's equations of a energy minimisation problem. There are at least two advantages in this approach arising from the fact that the unknowns of the problem are fluxes of $\vec{D}$, i.e. normal components of this vector: a) one can ensure strictly the Gauss's law when integrating on the surface of a tetrahedron, b) one get **automatically** the right continuity for normal component of $\vec{D}$ on interfaces between different media. In the following this finite element will be called "H(div)".

In a very similar manner one can define a finite element whose unknowns are circulations ( instead of fluxes) along edges of tetrahedras, ensuring Faraday's and Ampère's laws on each of them and the right continuities of tangential components. These elements will be called "H(curl)".

Combining these three kinds of elements the PRIAM/ANTIGONE code solves specific electromagnetic problems (electrostatics, magnetostatics, eigenmodes...) as well as the full time domain Maxwell problem.

## 4 STATIC DOMAIN

*Electrostatics*

The package offers the possibility of using both P1 or H(div) elements. The first one is recommended when the user is interested in getting good values for the potential. The second one is well suited in presence of different kind of dielectric materials ; this is especially true when one is interested in getting values of capacities.

*Magnetostatics*

H(curl) element is used in solving the magnetostatic problem with $\vec{H}$ as unknown:

$$\begin{aligned} curl\,\vec{H} &= \vec{j} \\ div(\mu\vec{H}) &= 0 \end{aligned} \qquad (9)$$

Although not yet programmed in PRIAM/ANTIGONE an other formulation is possible using a H(div) element solving the problem with $\vec{B}$ as unknown:

$$\begin{aligned} div\,\vec{B} &= 0 \\ curl\frac{\vec{B}}{\mu} &= \vec{j} \end{aligned} \qquad (10)$$

The choice between the two possibilities depends on whether one wishes to ensure the right continuity on interfaces for $\vec{H}$ or for $\vec{B}$.

## 5 FREQUENCY DOMAIN

In the frequency domain the mixed finite elements provide very attractive results. The HF eigenmode problem for the electric field $\vec{E}$ is :

$$\frac{1}{\varepsilon} curl \frac{1}{\mu} curl\vec{E} = \omega^2 \vec{E} \qquad (11)$$

with the boundary condition on conducting walls :

$$\vec{E} \times \vec{n} = 0$$

Obviously the H(curl) element is very well suited in solving this problem. The formulation provides values of the circulation of $\vec{E}$ along the edges of the tetrahedras. So it is straightforward to get values of the fluxes of magnetic field $\vec{B}$ on the faces of the tetrahedras through the relation :

$$\iint_F \vec{B}.\vec{n}\,dS = \frac{-1}{i\omega}\iint_F curl\vec{E}.\vec{n}\,dS = \frac{-1}{i\omega}\oint \vec{E}\,d\vec{s} = C_1 + C_2 + C_3 \qquad (12)$$

$C_1$, $C_2$, $C_3$ beeing the previously calculated value of the circulation of E along the 3 edges of the face F. A very interesting property of the method is that it **does not provide any "spurious" (or "parasitic") mode** unlike more classical approaches. In these latter the phenomenon seems to be due to the fact that these formulations do not ensure the divergence free condition for $\vec{D} = \varepsilon\vec{E}$. The H(curl) element leads intrinsically to a divergence free $\vec{D}$.

The vector $\vec{H}$ is solution of the same eigenvalue problem as $\vec{E}$ (but with "dual" boundary conditions). Both formulations (in E and in H) are implemented in ANTIGONE (3D). It can be shown that H-formulation approximates the frequency by upper values whereas the E-formulation approximates it by lower values. In this manner we can get a range within lies the exact value. It worth noting that in the 2D case the H-formulation is equivalent to the method used in the well-known program SUPERFISH.

In PRIAM/ANTIGONE quasi-periodic boundary conditions are implemented in addition to the classical ones.

In the 2D case it is possible to get "transverse modes" (dipoles,quadrupoles etc.) for an axisymmetric geometry.

## 6 TIME DOMAIN

The use of the H(div) and H(curl) element for spatial discretization can be coupled with a time scheme for solving evolutive problems described by the equations (1) and (2) rewritten under the form :

$$\frac{\partial \vec{D}}{\partial t} = \vec{j} - curl\, \vec{H}$$
$$\frac{\partial \vec{B}}{\partial t} = -curl\, \vec{E} \qquad (13)$$

PRIAM/ANTIGONE use a "leap-frog" scheme.

given $(curl\ \vec{E})^{n-1/2}$ and $\vec{B}^n$ at the time step n, the time step n+1 consists in the following :

- calculate the time derivative of the circulations of $\vec{E}$ along edges of the tetrahedras (H(curl) element) ;
- $(curl\, \vec{E})^{n+1/2} = (curl\, \vec{E})^{n-1/2} + \Delta t \frac{\dot{C}_1 + \dot{C}_2 + \dot{C}_3}{V}$ on each tetrahedron (volume V) ;
- $\vec{B}^{n+1} = \vec{B}^n - \Delta t (curl\, \vec{E})^{n+1/2}$.

This scheme is used with the driving term $\vec{j}$ equal to 0 (travelling waves calculations) or equal to a given function (wake field calculations). If particles are present in the structure, the driving term has to be estimated as we will see below.

The Maxwell's equations (3) and (4) are automatically satisfied if they are at the initial time.

In the time domain absorbing boundary conditions ("open" boundaries) are implemented, in addition to usual ones.

## 7 SELF-CONSISTENT CALCULATION WITH PARTICLES

In presence of a charged particle beam, the particles contribute to the the driving terms $\rho$ and $\vec{j}$. Such a beam is modelized by a set of macroparticles represented as Dirac distributions, so we have :

$$\rho = \sum_p q_p \delta(\vec{r} - \vec{r}_p)$$
$$\vec{j} = \sum_p q_p \delta(\vec{r} - \vec{r}_p) \vec{v}_p \qquad (14)$$

$q_p$, $r_p$, $v_p$ beeing respectively the charge, position and velocity of the macroparticle p. The Maxwell's equations are solved for each time step by the above described space discretization and time scheme. In the finite element formulation the Dirac distributions for the driving terms occur inside integrals and are regularized from this fact.

In addition to the Maxwell's equations we have to take into account the Newton-Lorentz equations for each macroparticle :

$$\frac{d}{dt}(\gamma \vec{\beta}_p) = \frac{e}{mc}(\vec{E} + c\vec{\beta}_p \times \vec{B}) \qquad (15)$$

(e,m charge and mass of the considered kind of particle ; c light velocity, $\beta_p$ ratio of the macroparticle velocity to c)

The time cycle of such a program consists of the following steps :

- solve the field equations (finite element method, here H(curl) element) with current positions and velocity of macroparticles ;
- from the field provided by the preceeding step, get the fields at the current positions of the macroparticles ;
- from these fields solve the Newton-Lorentz equation for each macroparticle (A Buneman-Boris algorithm is used) and update macroparticles positions and velocity.

The implementation includes the generation of particles at emitting surfaces following rectangular or gaussian pulse shape. Any shape is easily programmable.

Different initial conditions are available : electrostatic field, RF field etc. These fields are computed on the same mesh with the described above finite elements, avoiding any interpolation.

## 8 INTERFACES

The PRIAM/ANTIGONE package do not impose the use of determined mesh generators nor postprocessor. It can be interfaced with any finite element package or graphical software. At the moment interfaces with MODULEF, ANSYS, SYSTUS finite element mesh generators are available. Implement other interfaces is straightforward.

The code is written in standard FORTRAN-77 and therefore can be implemented on any system.

## 9 CONCLUSION

PRIAM/ANTIGONE offer a appreciable number of modules for solving the Maxwell's equations both in two and three dimensions, in static, frequency, time domains as well as in the particle coupled case. The package presents the advantage of using a consistent finite element formulation taking into account foundamental properties of the Maxwell's equation which can be interpreted in terms of continuities of field components.

Further developments are planed in the harmonic domain, especially S-matrix computation.

## 10 REFERENCES


[1] G. Le Meur, F. Touze, "PRIAM : a self consistent finite element code for particle simulation in electromagnetic fields", EPAC-90 (éd. Frontières)

[2] P.A. Raviart, J.M. Thomas, "a mixed finite element method for 2nd order elliptic problems", Lecture notes in Mathematics, vol 606, Springer, 1977

[3] J.C. Nédélec ,"mixed finite elements in $R^3$", Numerische Mathematik, 35, pp 315-341

[4] C. Travier et al. , M. Chanudet, This conference.

# The TESLA Test Facility Linac Injector

M. Bernard, J.C. Bourdon, R. Chehab, T. Garvey, B. Jacquemard, B. Mouton, M. Omeich, J. Rodier, P. Roudier, Y. Thiery,
Laboratoire de l'Accélérateur Linéaire, IN2P3 - CNRS, Orsay, France.

B. Aune, M. Desmons, J. Fusellier, J.F. Gournay, M. Jablonka, J.M. Joly, M. Juillard, A. Mosnier,
DAPNIA / SEA-CE, Saclay, France.

S. Buhler, T. Junquera,
Institut de Physique Nucléaire, IN2P3 - CNRS, Orsay, France.

*Abstract*

The TESLA Test Facility (TTF) Linac is a 500 MeV, 1.3 GHz superconducting accelerator under construction at DESY (Hamburg) by an international collaboration. The linac is being built to demonstrate the viability of the superconducting RF approach to a future $e^+e^-$ linear collider. Within the collaboration three participating French laboratories (LAL, IPN and DAPNIA) have undertaken the task of designing and constructing a phase 1 injector for TTF. We describe the studies towards the realisation of this 7 - 14 MeV, 8 mA high duty cycle (800 μs pulse, 10 Hz repetition rate) injector. The front end of the injector will consist of a 250 keV electron gun, a 216.7 MHz sub-harmonic bunching cavity and a superconducting capture cavity at the main linac frequency. This is followed by a beam analysis line and a transport section to match the beam from the capture cavity to the first cryomodule of the main linac.

## 1. INTRODUCTION

The TTF linac will essentially consist of an injector, four 12 m long cryomodules each containing eight 9 cell superconducting (SC) 1.3 GHz cavities of length 1.04 m, and a beam analysis line to measure the properties of the accelerated beam. To properly test such issues as HOM dissipation and wakefield excitation requires an injector capable of delivering a train of bunches with the characteristics of the TESLA proposal itself, i.e. $5 \times 10^{10}$ electrons per pulse at 1 MHz intervals during an 800 μs macro-pulse[1]. In contrast, the problems of operating high gradient (15 to 25 MV/m) SC cavities under high beam loading can be investigated using an injector capable of delivering the same average current albeit at reduced bunch charge and increased repetition rate. With this goal in mind we are constructing a 'phase 1' injector for TTF for which the specification is given in table 1.

Table 1
Specification of TTF phase 1 injector

| | |
|---|---|
| beam energy | > 5 MeV |
| average current | 8 mA |
| pulse length | 800 μs |
| bunch length | 1 mm (rms) |
| energy spread | < 1% (rms) |
| RMS emittance | 5 - 10 mm-mrad (normalised) |
| repetition rate | 10 Hz |

## 2. DESCRIPTION OF THE INJECTOR

The principal components of the injector consist of, (i) a triode electron gun capable of delivering micro-bunches with a variable frequency, (ii) a sub-harmonic bunching (SHB) cavity to provide longitudinal pre-bunching of the electron pulses, (iii) a superconducting 'capture cavity' to further bunch the electrons and to provide some pre-acceleration before injection into the linac, (iv) an analysis line to verify the correct adjustment of the beam parameters and (v) a transport section, consisting of two triplet magnets, to match the correctly adjusted beam to the main linac.

The bunch repetition frequency will be controlled by the application of fast (<1 ns) pulses to the gun cathode at the desired rate. The maximum rate of repetition is equal to the frequency of the SHB (216.7 MHz). At this frequency the 8 mA average current corresponds to bunch charges of 37 pC ($2.31 \times 10^8$ e's per pulse). For good pre-bunching the initial pulse-width should be sufficiently short in comparison with the period of the SHB and we set this to be 640 ps (± 25° of RF phase at 216.7 MHz) which corresponds to gun currents of 115 mA for 'triangular' pulses.

The choice of a superconducting structure (identical to those used in the cryomodules) for the capture cavity is influenced by the long macro-pulse width and consequent high average power that would be required of a copper structure to provide significant pre-acceleration of the beam coming from the gun. On the other hand, the leakage field of the SC cavity and the fact that it is not β-graded, necessitates the use of a gun producing electrons of energy superior to 200 keV.

### 2.1 *The Electron Gun*

The electron gun will be a modified triode gun, built by Hermosa Electronics (California), and originally employed on the ALS linac at Saclay[2]. After reduction of the anode-cathode spacing we have measured currents in excess of 500 mA at 30 kV. This is largely sufficient to provide the possibility of operating the injector at frequencies lower than 216.7 MHz. The additional energy of the beam will be provided by an electrostatic accelerating column capable of sustaining 300 kV in air, as is employed on the S-DALINAC at the TH Darmstadt[3]. Simulations of the injector using the PARMELA code indicate that we need to maintain the gun voltage to better than 0.1% during the 800 μs pulse if we wish to keep

the final beam parameters within the required specification. In order to do this we power the column via a 33 nF capacitor fed by a 300 kV - 1 mA power supply. The risk of electrical breakdown and the consequent release of stored energy in the system presents a major concern for the succesful operation of the injector. Simulations using the EGUN[4] code indicate that not all of the current available from the gun can be reasonably transported through the electrostatic column and so initial operation of the injector will be restricted to 216.7 MHz. However the installation of an 'Einzel' focusing lens at the input to the column holds the promise of increased bunch charge operation at a later date[5].

### 2.2 *The Sub-harmonic Buncher*

The frequency of the SHB cavity is chosen to be 1/6 of the frequency of the main accelerating cavities in order that its period is sufficiently larger than the gun pulse widths. This is required to ensure good pre-bunching of the beam and to avoid as much as possible the loss of electrons on the SC walls of the capture cavity. The SHB cavity consists of a single re-entrant cell and is fabricated from stainless steel. To provide the cavity with a high quality factor (Q = 24300) the inner walls of the cell will be coated with a thin (20 μm) deposition of copper. SUPERFISH calculations indicate that the cavity will have a transit-time corrected shunt impedance ($R_S = V^2/2P$) of 3.11 MΩ. The peak cavity Volts required to provide the necessary pre-bunching is calculated to be 50 keV leading to a modest peak power dissipation of 400 W. In order to provide some margin for safety the cavity will be powered using an RFTS (Bordeaux) amplifier, capable of delivering 2 kW pulses for up to 5 ms at 10 Hz. The amplifier is rated to have a phase stability of ± 0.5° and amplitude stability of ± 0.5% during a 1 ms pulse.

### 2.3 *The Capture Cavity*

The role of this cavity is twofold; (i) to terminate the bunching initiated upstream. The bunches will have a duration of < 100 ps at the entrance to the cavity and will be compressed by a further factor of 10, (ii) in addition this cavity will provide the necessary energy (7 - 14 MeV) for injection into the first cryomodule, the energy depending on the field at which the strucure is operated. The capture cavity is a standard TESLA cavity (9 cell, 1.3 GHz) identical to the 32 cavities of which the TTF linac is composed. It incorporates all of the new concepts developed for the TESLA project, i.e. the helium vessel integrated to the body of the cavity with a reduced LHe volume (25 liters), and with both the main and HOM couplers located in the cryostat vacuum. This cavity is installed in a special cryostat connected to the cryogenic distribution lines of the linac and is operated at 1.8 K. Although there is sufficient reserve power in the 4.5 MW klystrons which power the main linac cavities (1 klystron per 16 cavities) the capture cavity will be powered with its own individual 300 kW klystron. This will permit improved control of the klystron phase and amplitude thus simplifying the operation of the injector. It should be noted that, as for the main linac cavities, this structure will be operated in pulsed mode in contrast to other SC RF systems which accelerate continuous beams and are constantly powered with RF.

### 2.4 *Beam Diagnostics*

To verify that the beam has the required characteristics it is necessary to install appropriate instrumentation along the linac. A capacitive pick-up monitor will be used at the exit of the column to monitor the beam pulse from the gun. Current measurements elsewhere will be made with toroidal monitors, in particular, differential measurements of the current before and after the capture cavity will detect the presence of any beam losses and provide a signal to "trip-off" the gun. Beam position monitors (BPM) will be "button electrode" devices as employed at the ESRF[6]. An additional electrode on one BPM will allow a measurement of the RF phase of the beam with respect to the master-oscillator phase.

The transverse profile of the beam will be measured using retractable aluminium-oxide screens. Quantitative information on the horizontal beam profile will be obtained for the 250 keV beam using a secondary electron-emission monitor (SEM-grid). The low range of 250 keV electrons in suitable grid materials make the design of this monitor particularly delicate. A non-rotating magnetic lens upstream of the SEM-grid will enable the calculation of the beam emittance from measured profiles using the '3-gradient' technique.

The transverse profile of the beam after acceleration in the capture cavity will be measured using optical transition radiation (OTR) from a thin metallic foil placed in the beam path. As above, profile measurements for different settings of the first of the triplets will allow calculation of the emittance of the accelerated beam. In particular, the use of an image intensifier coupled to a CCD camera may permit time resolved emittance measurements of a small window (>100 ns) within the macro-pulse. Streak camera measurements of the OTR signal will permit measurement of the bunch length with 2 ps resolution. A second SEM-grid, placed at the focal plane of the bending magnet of the beam analysis line will measure the horizontal profile of the deviated beam thus allowing measurement of the energy dispersion. The SEM-grid will have forty tungsten wires of 0.1 mm diameter placed 2 mm apart and will provide an energy resolution of 0.1%. The vertical profile of the deviated beam will be measured using OTR.

Faraday cups, placed before the capture cavity and the first cryomodule, will be used during commisioning of the linac which will start cautiously with reduced pulse-widths of 10 μs, gradually building up to the full 800 μs pulse-width. X-ray monitors placed in the neighbourhood of beam collimators will provide an alarm in the event of beam scraping.

## 3. INJECTOR SIMULATIONS

We have performed extensive modelling of the injector beam dynamics from the exit of the electrostatic column to the entrance of the first cryomodule using the simulation code PARMELA[7]. Initial runs were used to optimise the distance from the SHB to the capture cavity for reasonable SHB field

amplitudes. The distance between the gun and the SHB is set to a minimum while still allowing space for appropriate elements (pumping, focusing, steering, diagnostics...). The simulation uses the electromagnetic fields of the capture cavity and SHB as calculated from their geometries using SUPERFISH. In the case of the capture cavity the important contribution of the leakage field is taken into account. The final layout of the injector is shown in figure 1. To maintain reasonable transverse beam sizes four magnetic lenses are employed between the gun exit and the entrance to the capture cavity cryostat, their positions and field strengths being optimised in the simulation.

At the time of writing the largest uncertainty among the beam parameters is the size and divergence of the beam which will emerge from the electrostatic column. We assume for the moment therefore, as reference input parameters to the code, a maximum beam radius of 2.5 mm, a maximum divergence of 6 mrad (edge emittance = 15 mm-mrad), an energy of 250 keV, a pulse-width of ± 150° at 1.3 GHz and a bunch population of $2.31 \times 10^8$. Initially we have used a capture cavity field corresponding to a maximum energy gain of 15 MV/m but our simulations show that equally good beam characteristics can be found for energy gains as low as 7MV/m. A lower RF field offers the advantage that the RF focusing effect of the cavity is reduced leading to a less divergent beam exiting the structure. This in turn makes the matching of the beam to the linac less sensitive to the setting of the triplets[8]. In addition the required performance of the capture cavity is easier to achieve. The simulations show that de-bunching of the beam in the long (6.36 m) transport section between the capture cavity and the linac is negligible for energy gains of 10 MV/m and we now take this value as our 'reference case'. The final beam characteristics at the exit of the capture cavity are shown in table 2 and can be seen to be compatible with the injector specification.

Table 2
Injector beam characteristics as calculated by PARMELA
(for capture cavity energy gain of 10 MV/m)

| | |
|---|---|
| Energy | 9.9 MeV |
| RMS phase width | 0.77° |
| Total phase width | 3.2° |
| RMS bunch length | 0.49 mm |
| RMS energy spread | 78 keV |
| Total energy spread | 300 keV |
| Relative energy spread (rms) | 0.8% |
| Norm. rms emittance (both planes) | 4.2 mm-mrad |

## 4. ACKNOWLEDGEMENTS

We are indebted to many of our fellow TESLA collaborators for discussions regarding the injector in the course of numerous TTF workshops and meetings.

## 5. REFERENCES

[1] B. Dunham and M. Jablonka, "Modelling of a High Charge Injector for the TESLA Test Facility", these proceedings.
[2] B. Aune et. al., "Improvement of the Electron Injection for the ALS Electron Linac", Proc. of the Linear Accelerator Conference, California, USA, SLAC report 303, 1986.
[3] H. Genz et. al., "Operational Experience and Results from the S-DALINAC, Proceedings of EPAC 92, Berlin, FRG, March 1992, pp 49-51.
[4] W.B. Herrmansfeldt, "EGUN - An Electron Optics and Gun Design Program", SLAC report 331, 1988.
[5] J. Chaumont, private communication.
[6] K.Scheidt and F. Loyer, "Synchrotron Injector Beam Position Monitor System", Proceedings of EPAC 92, Berlin, FRG, March 1992, pp 1121-1123.
[7] We use a version of the original PARMELA code which has undergone some revision. See B. Mouton, LAL/SERA 93-455, September 1993.
[8] H. Weise, private communication.

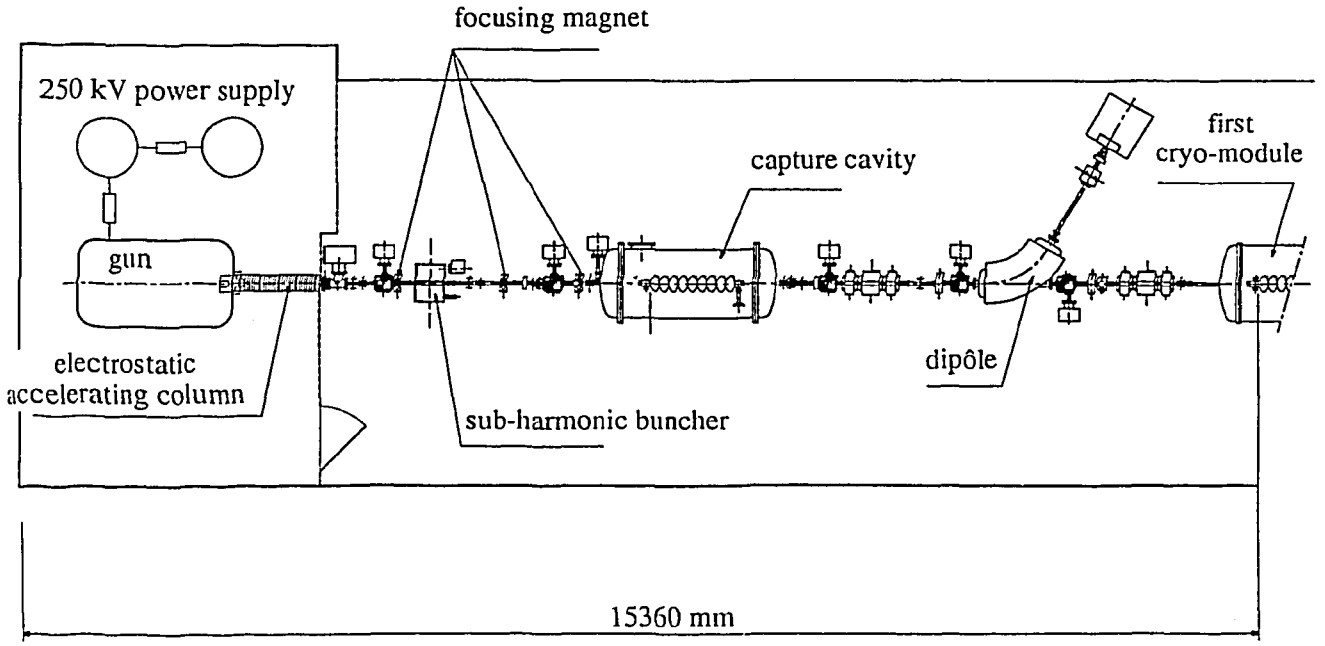


Figure 1. Schematic Layout of TTF Injector.

# On some RF Three-dimensional Simulations of Magnetically Coupled Cells

Marie Chanudet
Laboratoire de l'Accélérateur Linéaire
IN2P3-CNRS et Université Paris-Sud,
Centre d'Orsay, 91405 ORSAY Cedex, France

*Abstract*

The study of an accelerating structure, without cylindrical symmetry, by means of a 3-D electromagnetic code gives a better knowledge of the electromagnetic properties of the structure. In particular its allows to compute some important RF characteristics for comparison with either analytical method or prototype measurement.

## 1 INTRODUCTION

In a backward travelling wave structure, the cells are magnetically coupled through some small apertures located out off the axis. Then the cylindrical symmetry is broken and to entirely simulate the electromagnetic field, 3-D computer codes are necessary. The package ANTIGONE (3-D) [1] was used to calculate resonant modes. The present study deals with a particular S band accelerating section operating at $3\pi/4$ mode in which the magnetically coupled cells have different geometries without smooth transition between low field cells and high field cells with longer noses (see figure 1).

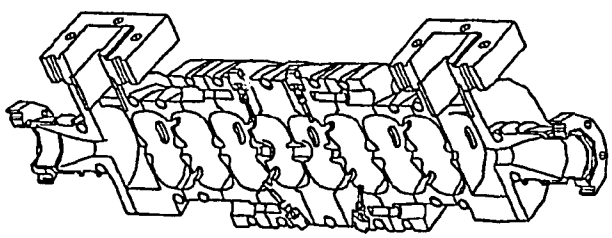

Figure 1: The backward wave section MECCANO

First, the two types of cells are studied separately. When the magnetic coupling holes between the cells are meshed, the program gives directly the frequencies, dispersion curve and coupling coefficient for the fundamental mode as well as for higher order modes. If the coupling aperture is not meshed, an analytical approach also permits to calculate the coupling coefficient [2] and to compare it to the foregoing simulations. Several significant RF characteristics are determined for every cell, for instance three methods to find the effective shunt impedance in the case of a phase advance per cell of $3\pi/4$ are proposed, performed and compared.

## 2 COUPLING BETWEEN CELLS

For each type of geometry, a three-dimensional mesh composed of tetrahedrons of various dimensions describes two half volumes joined by the coupling apertures and beam tube. To limit the number of mesh points, only one quarter of the cavity in the azimuthal direction is generated.

### 2.1 Dispersion Curve

With Neuman boundary conditions, the code ANTIGONE can, of course, calculate the 0 and $\pi$ modes. Moreover, the phase advance can be forced between identical extremal planes of the cavity. So, one single cavity is sufficient to compute precisely the frequency variations with the phase advance. This program also provides two methods of resolution: the E or B formulation. The wave equation applied to the electric field E (or magnetic field B) is numerically solved in determining the E (or B) flux along the mesh lines. Once E (or B) are calculated, the complementary components B (or E) are deducted from the Maxwell's mixed equations [1]. Two different dispersion curves calculated from E and B formulations are shown in figure 2, where the measured dispersion curve is just sitting in between.

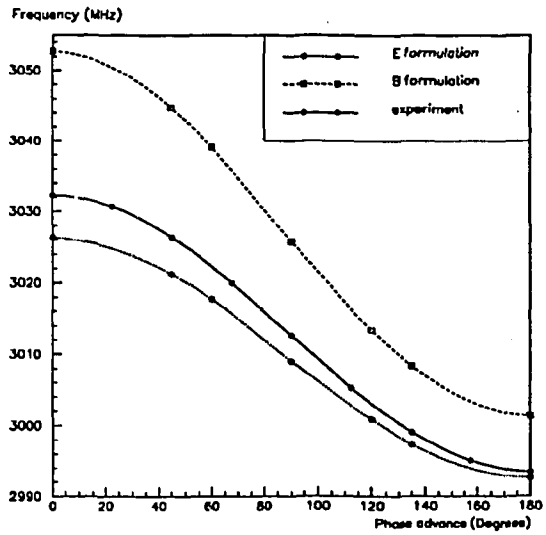


Figure 2: Dispersion curves of the low field cavity

These data also are correctly fitted by the classical formula of dispersion

$$\omega_\theta^2 = \omega_{\pi/2}^2 \, (1 + k cos\theta) \qquad (1)$$

where $\theta$ is the phase advance per cell, $\omega_\theta$ is the corresponding angular frequency and $k$ is the coupling coefficient (if $k > 0$ the coupling is mainly magnetic, if $k < 0$ it is electric).

## 2.2 First Passbands

The first modes of the two types of cells have been simulated and compared to $TM_{nml}$ and $TE_{nml}$ modes of cylindrical cavities. Since the used meshes describe only one quarter of the cell, they are delimited by two perpendicular planes containing the mechanical axis. Each plane is treated by the code as a boundary condition (B.C.) of either metallic or symmetric. This choice implies a fictive polarization of the field in the cell. If the two planes are metallic (mm), the field variations with the azimuthal angle $\phi$ are $cos(n\phi)$ or $sin(n\phi)$ like with $n$ even; then only the $TM_{nml}$ modes with $n$ even are calculated. If the planes are different, and either the metallic one cuts the coupling aperture (ms) or does not (sm), only the $TM_{nml}$ modes with $n$ odd are found. For frequencies less than 7000MHz the results computed with E formulation are shown in table 1.

Table 1: First modes for high and low field cells

| Modes | B.C. | High field cell | | Low field cell | |
|---|---|---|---|---|---|
| | | $f_{\pi/2}$ MHz | $k$ $\times 10^{-3}$ | $f_{\pi/2}$ MHz | $k$ $\times 10^{-3}$ |
| $TM_{010}$ | ss | 2988.93 | 9.39 | 3008.98 | 11.22 |
| $TM_{110}$ | sm | 5534.31 | 5.30 | 5056.45 | 11.40 |
| $TM_{110}$ | ms | 5547.55 | 2.06 | 5085.60 | 0.24 |
| $TM_{210}$ | ss | 7317.36 | -1.04 | 6599.38 | 3.81 |
| $TM_{020}$ | ss | 6808.68 | 3.93 | 6781.45 | 2.47 |

For the two types of cell, the same $TM_{nml}$ modes appear in the same order as with a perfectly cylindrical cavity, all except the inversion of $TM_{020}$ and $TM_{210}$ modes for the high field cell. The explanation is that the introduction of a metallic nose in an electric field decreases the resonant frequency and the larger are its dimensions and the magnitude of the E field, the stronger is the variation.

## 2.3 Semi-analytical approach

The coupling coefficient in equation (1) can be also deduced from a perturbative method [2]. Opening an aperture in a cavity creates a shift of the resonant frequency. If the aperture has an elliptical shape of small dimensions compared to the wave length and if the electromagnetic field is uniform on this region, the new frequency can be calculated. In the case of a phase advance per cell equals to $\theta$, the new frequency becomes

$$\begin{aligned}\frac{f^2}{f_0^2} = 1 &+ 2N\frac{\pi(1-e_0^2)\,l_1^3}{12\,E(e_0)}\,\frac{\varepsilon_0 E_3^2}{U}\,(1-cos\theta\; e^{-\alpha_3 b}) \\ &-2N\frac{\pi e_0^2\,l_1^3}{12[K(e_0)-E(e_0)]}\,\frac{B_1^2}{\mu_0 U}\,(1-cos\theta\; e^{-\alpha_1 b}) \\ &-2N\frac{\pi(1-e_0^2)\,l_1^3}{12[E(e_0)-(1-e_0^2)K(e_0)]}\,\frac{B_2^2}{\mu_0 U}\,(1-cos\theta\; e^{-\alpha_2 b})\end{aligned} \qquad (2)$$

where $f_0$ is the resonant frequency of the cavity without aperture, $N$ the number of similar apertures opened in the cavity, $b$ the depth of the coupling aperture, $2l_1$ and $2l_2$ the lengths of the major and minor axes of the elliptical aperture, $e_0 = (1 - l_2^2/l_1^2)^{1/2}$, $K(e_0)$ and $E(e_0)$ the elliptical integrals of the first and second kinds, $E_3$, $B_1$ and $B_2$ the fields on the metallic walls at the center of the coupling apertures before they are opened (see figure 3), $U$ the stored energy in the cavity and $\alpha_1$, $\alpha_2$, $\alpha_3$ the attenuation coefficients inside the aperture.

The results obtained with E formulation for the high field type of cell when the coupling aperture is not meshed are given in table 2. A reason of the discrepancy of these values with 3-D simulation ones is that the numerical calculations are not very accurate. In the case of high order modes, the difference is larger than for the fundamental because the field varies more rapidly with $r$ and $\phi$ and the hypothesis that the fields are uniform over the region of the coupling aperture becomes wrong.

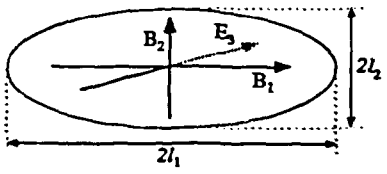


Figure 3: Elliptical aperture and the $E_3$, $B_1$, $B_2$ fields

Table 2: Analytical method for high field cell

| Modes | B.C. | $E_3$,$B_1$,$B_2$ av. | | $E_3$,$B_1$,$B_2$ max. | |
|---|---|---|---|---|---|
| | | $f_{\pi/2}$ MHz | $k$ $\times 10^{-3}$ | $f_{\pi/2}$ MHz | $k$ $\times 10^{-3}$ |
| $TM_{010}$ | ss | 2976.44 | 8.45 | 2974.54 | 9.58 |
| $TM_{110}$ | sm | 5562.52 | 0.88 | 5558.79 | 3.51 |
| $TM_{110}$ | ms | 5547.51 | 1.39 | 5542.22 | 1.48 |
| $TM_{020}$ | ss | 6831.51 | 0.61 | 6813.28 | 4.77 |
| $TM_{210}$ | ss | 7319.29 | -1.18 | 7321.28 | -1.16 |

# 3 SHUNT IMPEDANCE

If the 3-D code well simulates the magnetic coupling, the knowledge of the electromagnetic field, the energy stored in the cavity and the losses in the walls will allow to determine the magnitude of the effective shunt impedance. It is usually expressed as:

$$r = \frac{(\int_0^l e_z\, dz)^2}{l\, P_{0-l}} \qquad (3)$$

where r is the effective shunt impedance per unit length, $l$ is the section length, $e_z$ is the electric field seen by the particle and $P_{0-l}$ is the power lost along the distance $l$. Since the structure operates in a travelling wave with a phase advance of $3\pi/4$ per cell and since the program computes standing waves, three methods to calculate the effective shunt impedance of the $3\pi/4$ mode are proposed, with the aim of limiting the number of mesh points.

## 3.1 From $3\pi/4$ mode with two cells

The phase advance per cell being equal to $3\pi/4$, it becomes $3\pi/2$ for two cells and the $3\pi/4$ mode can be obtained by generating a mesh with only two cells and setting the boundary conditions either symmetric or metallic at the

end planes. Using the properties of the waves in a periodic structure for $\theta = 3\pi/4$ and the previous boundary conditions, the equation (3) after a simple calculation becomes

$$r^{tw} = 2\,\frac{(E_{z0}/2)^2\,2d}{P^{sw}_{0-2d}} \qquad (4)$$

where $tw$ indicates the travelling wave and $sw$ the standing one, $E_{z0}$ is the fundamental amplitude of the stationary wave, $d$ the length of one cell and $P^{sw}_{0-2d}$ the wall losses for the two cells.

### 3.2 *From $3\pi/4$ mode with one cell*

Another method using the possibility to set the $3\pi/4$ phase advance between two identical planes of a single cell and the expansion in space harmonics of the magnetic field has also been performed [3]. Corresponding results are shown in table 3.

### 3.3 *From $\pi$ mode*

As the diameter of the iris of the cells is small (<7.mm), the electric field on the axis is very small at the location of the iris. In the first half volume the electric field pattern $E^{\pi}_z$ of the $\pi$ mode is similar to that of the $3\pi/4$ mode. The electric field $E_z$ of the $3\pi/4$ mode is then reconstituted along the two cells with the relations:

$E_z(z)=E^{\pi}_z(z)$ if $0 < z < d/2$,
$E_z(z)=cos(3\pi/4) * E^{\pi}_z(d-z)$ if $d/2 < z < d$,
$E_z(z)=cos(3\pi/4) * E^{\pi}_z(z-d)$ if $d < z < 3d/2$,
$E_z(z)=0$ if $3d/2 < z < 2d$.

Assuming the losses are proportional to the square of $E_z$, they are approximated for $3\pi/4$ mode by $P_{0-2d} \simeq 2\ P^{sw\ \pi}_{0-d/2}$. Finally, the shunt impedance becomes equal to

$$r^{tw} \simeq 2\,\frac{(E_{z0}/2)^2\,2d}{2P^{sw\ \pi}_{0-d/2}}. \qquad (5)$$

### 3.4 *Validity*

The calculated shunt impedances are presented in table 3. The three methods are validated by the fact that the maximum difference of 7% between the different results is less than the estimated measurement error of 10%. They should be generalized to other values of phase advance. The method using two cells appears as the most natural and is surely the most accurate because it uses a formula without approximation. Moreover, the $\pi$ mode is very simple and gives a good performance although rough approximation is used.

Table 3: Shunt impedance for the high field cell

| form. | method | | $E_{z0}$ | $P_{0-2d}$ | $r^{tw}$ |
|---|---|---|---|---|---|
| | mode | nb cell | MV/m | W | MΩ/m |
| E | $3\pi/4$ | 2 | 0.547 | 25.90 | 108.52 |
| | $\pi$ | 1 | 0.546 | 26.05 | 107.39 |
| B | $3\pi/4$ | 2 | 0.596 | 29.07 | 114.6 |
| | $3\pi/4$ | 1 | 0.597 | 29.11 | 114.98 |
| | $\pi$ | 1 | 0.597 | 29.63 | 112.7 |

## 4 OTHER RF CHARACTERISTICS

A more complete analysis of the simulations gives additional RF characteristics for the accelerating structure such as the quality factor Q, the group velocity $v_g$ or the attenuation coefficient $\alpha$. The simulated and measured values appear to be in very good agreement as shown in table 4.

The visualization of the electromagnetic field in all the meshed volume allows the study of the problem as a whole. So, the variations of the field may be observed (particularly the points of maximum electric amplitude on the metallic surface.)

Table 4: RF characteristics for the low field cell

| | $f_{3\pi/4}$ MHz | $k$ $\times 10^{-3}$ | Q | $c/v_g$ | $r^{tw}$ MΩ/m | $\alpha$ Nep. |
|---|---|---|---|---|---|---|
| Sim. | 2997.02 | 11.2 | 1300 | 104 | 95 | 0.12 |
| Exp. | 2998.07 | 12.7 | - | 94 | 93 | 0.11 |

## 5 CONCLUSION

The computer simulations of a magnetically coupled structure made of different cell geometries (low field and high field volumes) have shown that the 3-D code ANTIGONE is quite well suited due to its ability of setting the phase advance per cell and because it offers the two types of field formulations (E and B). Consequently the difficulties of a 3-D meshing for long structures together with the time consumption are partly overcome.

## 6 ACKNOWLEDGEMENTS

I would like to thanks G. Bienvenue, P. Brunet, J. Gao, J. Le Duff, G. Le Meur and F. Touze for constant help or support.

## 7 REFERENCES

[1] G. Le Meur and F. Touze, "PRIAM/ANTIGONE: A 2D/3D Package For Accelerator Design", these proceedings.

[2] J. Gao, "Analytical formulas for the resonant frequency changes due to opening apertures on cavity walls", Nucl. Instr. and Meth., A311(1992) 437-443.

[3] M. Chanudet, "Simulations 3-D de la Cavité Fort Champ de la Section MECCANO", (Internal Note LAL, SERA 93-519, Sept. 1993)

# Dark Current under Low and High Electric Field.

G.Bienvenu P.Brunet
LABORATOIRE de L'ACCELERATEUR LINEAIRE D'ORSAY.
LAL Bat 201 service SERA
91405 ORSAY FRANCE

*Abstract*

Using CERN/LIL type cells an one meter long high temperature brazed, S band travelling wave section has been tested in our high power test facility NEPAL. In order to provide data for S band linear collider (SBLC), we have systematically investigated the characteristics of the dark current from this structure under low electric field conditions (less than 20 MV/m). We show that spectrum peaks are close to the nominal energy of the section so that dark current may be transmitted from section to section. An overview of experimental set-up and method of measurement of very low self-emitted current is described. the spectrum chape is discussed.
A beam has also been accelerated under high electric field conditions, the structure being fed through a peak power multiplier (SLED type).

## 1 INTRODUCTION TO LOW ELECTRIC FIELD CONDITIONS

In accelerating structures running under low electric field - lower than 20 MV/m - dark current is generally disregarded. If a long multi-section linac is proposed (SBLC) the dark current will be transmitted from section to section. At the end of the machine, the value of self emitted current may grow-up enough to disturb the main beam. In order to characterize the flow of field emitted electrons the measurement of an extremely low current is required. This problem is cleared-up by an electron counting system usually dedicated in particle physics domain.

## 2 ORIGIN OF DARK CURRENT UNDER LOW FIELD

Electrons pulled out from cavity surface, give a beam, for all phase conditions, if the strength of accelerating field reaches the critical value $E_c$:

$$k\pi < \frac{eE_c\lambda_\eta}{m_0c^2}$$

where k is a factor dependant of the intern shape of cells. usually $k \simeq 2$[1] so that for an S band structure:

$$E_c > 30MVm^{-1}$$

If the field is lower than $E_c$, dark current is not directly yielded by field emitted electrons, but by secondary electrons, like it is reported on simulation [2] of figure 1.

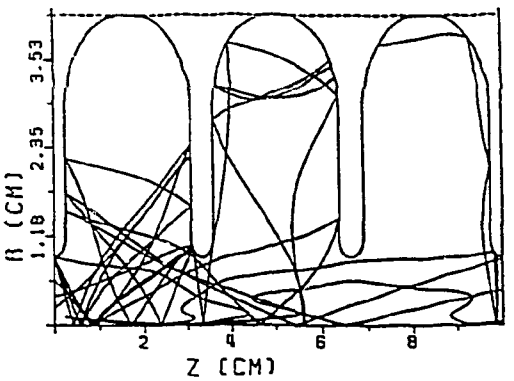


Figure 1: Simulation of dark current under low field

## 3 EXPERIMENTAL SECTION

The experimental section SERA/LIL-2 is an one meter long S band TW element. It is derived of our work on LIL structures [3]. Contrary to LIL technic cells are assembled by high temperature brazing. Mains characteristics of section are given by the table 1.

Table 1: experimental section parameters

| | |
|---|---|
| Nominal frequency | 2998.55 MHz |
| Total length | 1.10 $m$ |
| Number of cells | 30 |
| Shunt impedance | 70 $M\Omega m^{-1}$ |
| Attenuation | 3.0 $dB$ |
| Filling time | 0.55 $\mu s$ |
| Energy gain | $6.2\sqrt{P_{MW}}$ $MeV$ |

## 4 MEASUREMENT CONDITIONS

The sketch of experimental set-up is reported on the figure 2. The section is fed by a 3 $\mu s$ RF pulse with a 100 $Hz$. repetition rate.
The collimator input aperture is fixed at : $5X5$ $mm^2$ and the image slit of spectrometer is opened at 0.4 $mm$

## 5 COUNT DEVICE

Three plastic scintillators $S_1$ $S_2$ $S_3$ are set on the deviated way of spectrometer axis, as is reported on the figure 3.

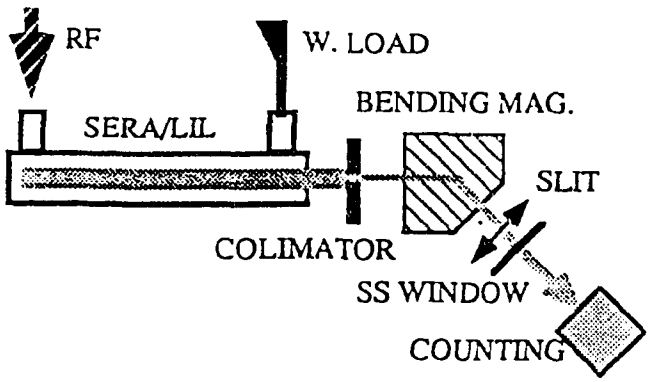


Figure 2: Measurement set-up

Gains of photomultipliers are equal, their signals are sent to three discriminators which give 5 $ns$ pulses . A RF synchronous signal is injected into the gate G.
An event is considered as good if:

$$\frac{(S_1 \bigcap S_2) \bigcap S_3}{(S_1 \bigcap S_2)} > 0.6$$

For an adequate statistics, the counting time has been fixed at 100 $s$.

## 6 RESULTS

Spectrums of figure 4 has been respectively recorded at the beginning of experiment and after 3 h of continuous running. The average accelerating field is 16.4 $MVm^{-1}$ and the theoretical maximum gain is $U_{Max} = 18\ MeV$ After 3 h the dark current amplitude decreases by about 10%. After a break, the initial intensity level is found again. On the figure 5 is reported the time dependence of the self emitted current, this bargraph is the sum of spectrums, recorded at various moments into the RF pulse (with a path of 0.5 $\mu s$). .

### *6.1 Charge and intensity*

Under our conditions, the electric charge and the peak current are respectively:

$$Q = 0.2\ fC$$

$$I = 60\ pA$$

## 7 SPECTRUM SHAPE

In a constant impedance structure, the surface field decreases all along of the section, so that the number of emitted electrons (respectively the number of secondary electrons) decreases versus the RF Fowller-Nordheim law. As electrons are rapidly relativistic their energy gain is directly dependent of their emitted point.The spectrum peak is maximum for the maximum energy gain (18 $MeV$) and decreases exponentially in accordance with experimental records.

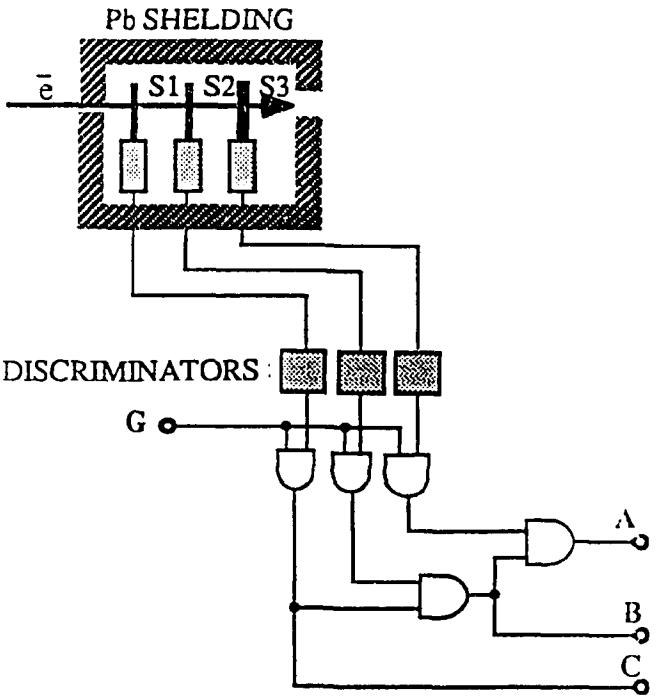


Figure 3: Counting device

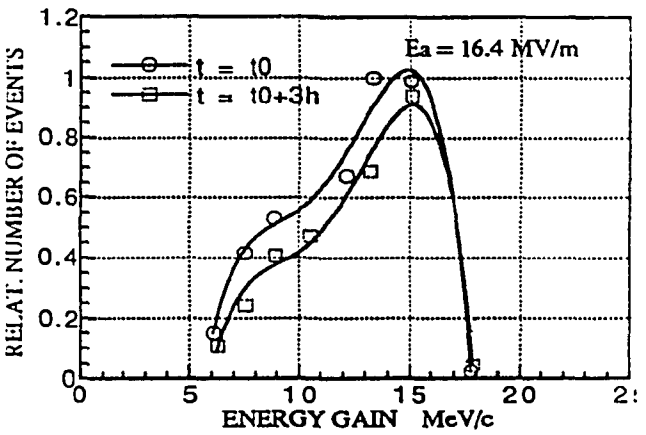


Figure 4: Spectrums of dark current

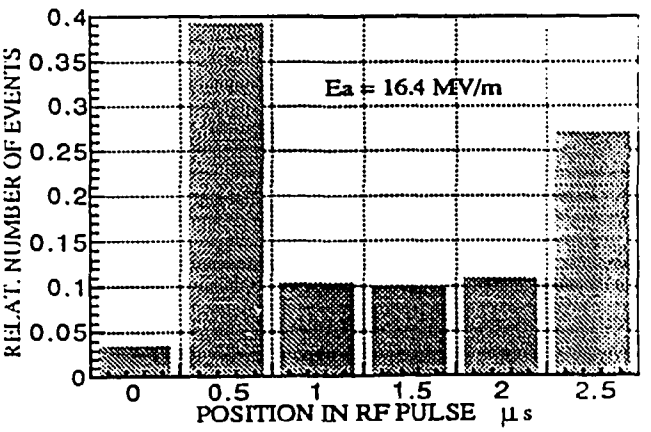


Figure 5: Time dependance of dark current

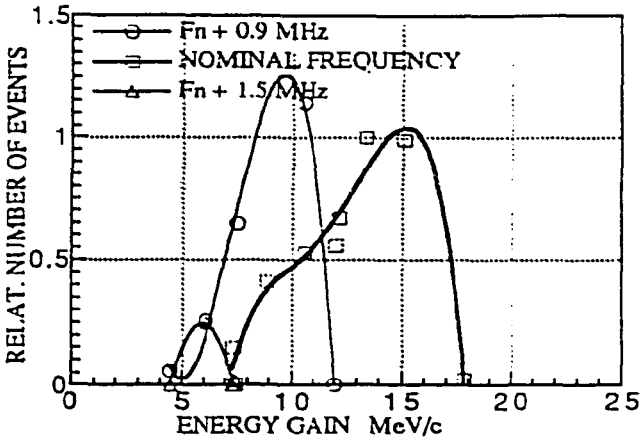


Figure 6: Relative number of events versus frequency

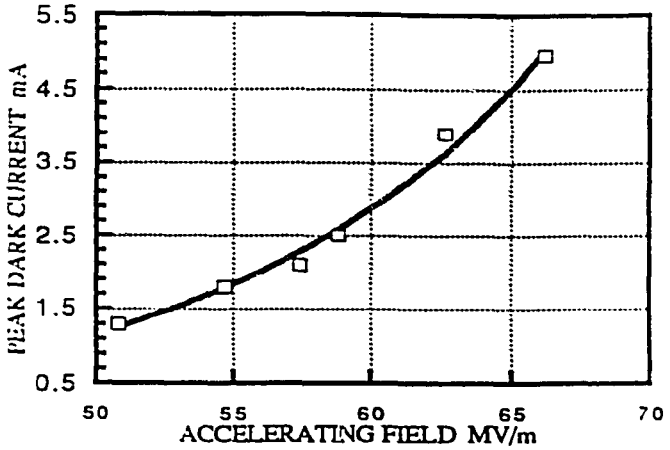


Figure 7: Dark current intensity in compressed mode

## 8 FREQUENCY DEPENDANCE

The consequence of a increase in the RF frequency has been also investigated in a narrow band around the nominal frequency ($F_n = 2998.55\ MHz$). Results are reported on the figure 6. The maximum intensity of dark current is obtained for $F = F_n + 0.9\ MHz$ (gain of 30%), consecutively the maximum energy decreases as far as 12 $MeV$.

## 9 HIGH ELECTRIC FIELD CONDITIONS

The main RF source of NEPAL supplies a 35 $MW$ rectangular pulse of 4.5 $\mu s$ length. It is also possible to feed the structure by a compressed pulse (SLED). In this case the buncher is connected to an auxiliary RF source of 4 $MW$. In compressed mode the available peak power is about of 210 $MW$

### 9.1 Rectangular pulses

With rectangular pulses, it is possible to feed our section at the nominal work conditions of the main klystron. For 35 $MW$ the accelerating field reach 40 $MVm^{-1}$. Unfortunately the level of the dark current is too high to be measured by the device described in 5 and too low for a direct measurement by a faraday-cup located at the direct output port of spectrometer.

### 9.2 Compressed pulses

In compressed mode the intensity of dark current is enough high for a measurement by means of torroïd transformer set at the end of deviated way.
The peak dark current intensity versus the average accelerating field is reported on the figure 7, for a 0.8 $\mu s$ compressed pulse.

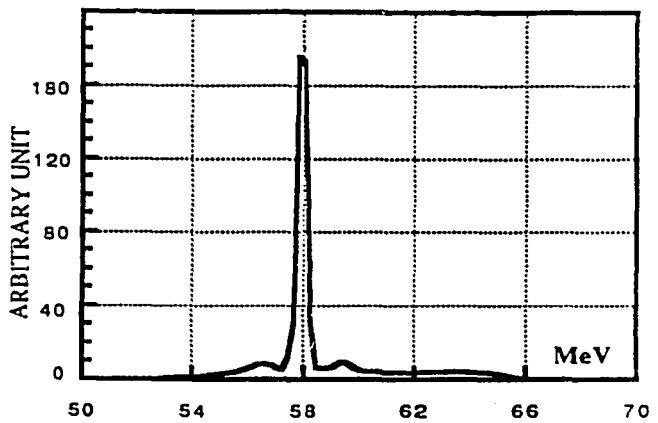


Figure 8: Accelerated current spectrum

## 10 ACCELERATED ELECTRON BEAM

Two moving plungers, located into the SLED cavities, allow us to switch easily from a SLED RF type pulse to a rectangular pulse. In this two cases, for radiation safety reasons, the repetition rate is decreased at 25 $Hz$.
The compressed pulse mode has bean used for accelerating routinely an electron beam of 600 $mA$ as far as 58 $MeV$. The energy spectrum is reported on the figure 8. After subtracting the thermïonic gun and buncher gain the energy gain for our SERA/LIL-2 section is:
54 $MeV$ per meter

## 11 REFERENCES

[1] G.Bienvenu, Mesure et étude de l'auto-émission électronique et du champ électrique des sections accélératrices d'électrons,LAL/RT 93-17 Nov 93

[2] P.Fernandes, Proceeding of Linear Accelerator Conference, 1988 Stanford p. 330

[3] R.Belbéoch et coll, Rapport d'étude sur le projet des linacs injecteurs de LEP (LIL), LAL/RT 82-01 Jan 82

# A Versatile TBA Lattice for a Tau-Charm Factory with and without Beam Monochromatization

A. Faus-Golfe* and J. Le Duff
Laboratoire de l'Accélérateur Linéaire
Centre d'Orsay Bat. 200, 91405 Orsay FRANCE

*Abstract*

Optics for a high luminosity $e^+e^-$ collider at a CM energy of 4 GeV with and without monochromatization of beams and achromatic TBA cells in the arcs have been carefully studied, including chromaticities correction, dynamic apertures and beam lifetime.

## 1 LUMINOSITY AND BASIC PARAMETERS CHOICES

The choice of the basic parameters has been done in two steps considering successively a standard optics and a monochromator optics.

In the case of a standard optics we will use a conventional flat horizontal beam collision optics without dispersion at the interaction point, IP. From [1] we can deduce that high luminosity will be obtained with $\beta_y^* \simeq 0.01$ m, a minimum bunch spacing $S_b \simeq 12$ m, and a large emittance $\epsilon_x$, provided the necessary beam current, $I_b$, can be achieved. At 2.0 GeV per beam, to obtain $L = 10^{33}$ cm$^{-2}$ s$^{-1}$, the emittance has to attain the value $\epsilon_x = 3.0\ 10^{-7}$ m rad.

In the case of beam monochromatization, positrons with energy $E_0(1+\varepsilon)$ colliding with electrons at $E_0(1-\varepsilon)$ and vice-versa are needed. In that case the CM energy resolution, $\sigma_w$, is reduced while the effective luminosity is increased [2]. This will be achieved by means of opposite vertical dispersions at IP for the two beams ($D_{y+}^* = -D_{y-}^* = D_y^*$). If we consider the introduction of vertical dispersion as the only modification of the usual flat beam scheme ($\sigma_x^* \gg \sigma_y^*, \beta_x^* \gg \beta_y^*$), it has been shown in [3] that this procedure leads to a gain factor $\lambda$ in the energy resolution and a loss in total luminosity by the same factor. If we take a horizontal flat beam with finite vertical dispersion at the IP, the vertical beam size is dominated by the beam energy spread $\sigma_\epsilon$, ($\sigma_y^* \simeq \sigma_\epsilon D_y^*$). Consequently the beam space charge parameter $\xi_y \ll \xi_x = \xi_{max}$. The reduction in luminosity can be compensated by a reduction of $\beta_x^*$ [4]. For practical reasons a small $\beta_x^*$ supposes a larger $\beta_y^*$. This inversion is only valid if we keep $\xi_x = \xi_{max}$, and that supposes a reduction in horizontal emittance ($\sigma_x^* \ll \sigma_y^*$). Under these conditions we can achieve a factor $\lambda$ in energy resolution without loss in total luminosity. According to beam-beam studies using finite dispersion at the IP [5], and assuming $D_y^* \neq 0$ and $D_x^* = 0$, we get a condition on the vertical beam-beam parameter $\xi_y \simeq 0.015$, together with a normal condition on the horizontal beam-beam parameter $\xi_x \leq 0.04$. Let's assume that $\beta_x^* = 0.01$ m and $\xi_x = 0.04$. At $E_0 = 2.0$ GeV per beam for keeping the luminosity at the level of 1.0 $10^{33}$ cm$^{-2}$ s$^{-1}$ with a colliding frequency $k_b f_r$=25 MHz, the number of particles per bunch must be $N_b$=1.2 $10^{11}$ and the horizontal emittance $\epsilon_x \leq 2.2\ 10^{-8}$ m rad. We can conclude in the case of an optimized monochromator optics, that the parameters choice is very different from the case of a standard optics.

*On leave from IFIC, Univ. of Valencia-CSIC

## 2 DESIGNING A VERSATILE COLLIDER

The Tau-Charm Factory (TCF) is a double ring with head-on collisions and electrostatic vertical separation scheme. In the following we describe the three main parts of the accelerator: the arcs, the insertion region (including the low-$\beta$ insertion and the slopes) and the utility straight section.

### 2.1 Arcs and emittances

Most of TCF designs have used conventional FODO cells in the arcs. The passage from low to high emittance is obtained by means of a special design of the standard arc cells. The emittances can be further reduced or increased with the help of Robinson, damping or emittance wigglers [4] [6].

In our study the original idea is based on low emittance lattices designed for the 3$^{rd}$ generation synchrotron radiation storage rings. At 2.0 GeV these emittances are typically of the order of $10^{-8}$ m rad.

These lattices are constructed from basic achromatic cells. In this context, achromatic means that the dispersion function is zero at the entrance and exit of the cells. Two parallel studies with two kinds of cells, namely Double Bend Achromat (DBA) and Triple Bend Achromat (TBA), have been made [7]. The procedure followed in both studies is the same. We can deduce from [8] that the TBA lattice gives better performances than the DBA lattice. So in the following we will concentrate on the TBA lattice only.

In the first part of the study we have designed the low-emittance arc (2.0 $10^{-8}$ m rad) essentially by choosing the right number of TBA cells. The change from low to high emittance (3.0 $10^{-7}$ m rad) is achieved by displacing and increasing the $\beta_{xmin}$ in the magnets. To get these conditions we decrease the strength of the quadrupoles in the achromat and allow the dispersion to be non-zero at

the ends of the module, to achieve a large contribution to the emittance. The optics of high and low emittance versions of these basic modules,matched with the codes BETA and MAD, are shown in figure 1. The dispersion for the high emittance case is finally suppressed at both extremities of each arc by a special matching of the last module, as shown in figure 1(b).

### 2.2 *Interaction region*

In this study the interaction region is designed in a more conventional way. It is essentially composed of a micro-$\beta$ insertion and a separation scheme.

To achieve in the two modes of operation a low-$\beta$ ($\beta_x^* \simeq 0.01$ m with monochromatization, $\beta_y^* \simeq 0.01$ m in the standard case) we use a superconducting doublet. The distance between the first superconducting quadrupole and the IP is kept at 0.8 m to locate the detector and to match easily both optics. However the distance between the first and second quadrupoles has been reduced from 1.0 to 0.5 m [4] [6] to avoid the growth of the high $\beta$-function, which is responsible for the high chromaticity in this kind of lattices.

The passage from monochromatization to standard scheme has been obtained freezing the location of the superconducting doublet and vertical dipoles and having additional quadrupoles in the sloping region. The figure 1 shows the optics for the two modes of operation.

### 2.3 *Utility insertion*

The double ring scheme has only one crossing point, hence the opposite insertion is made of two long straight sections corresponding to the two rings, with an equivalent length to the sloping insertion region.

The straight section is made of regular FODO cells without dipoles, leaving enough space to house RF cavities, beam instrumentation devices and additional sextupoles. These sextupoles will help the correction of chromaticities if necessary. The quadrupoles of this region are used to adjust the tunes ($Q_x$, $Q_y$) and make other compensations.

### 2.4 *Collider performances*

The performances for the TBA lattice are given in table 1. In this table we have included also the values of natural chromaticities, $Q'_{x,y}$, the strength of sextupoles, ($SF$, $SD$), and the maximum stable betatron amplitudes, $A_{x,y}$. To calculate the chromaticities and the sextupoles strengths we have used the HARMON module of MAD. To estimate the quality of this correction we have tracked the particles with $\delta$=0 during $10^3$ turns with MAD. We have obtained the maximum stable betatron amplitudes in both planes, i.e. $A_x$(with $A_y$=0) and $A_y$(with $A_x$=0), where $A_{x,y} = \frac{(x^*,y^*)^2}{\beta^*_{x,y}}$, as a function of sextupoles positions and tunes ($Q_x$, $Q_y$). To adjust the tunes we have used the quadrupoles of the FODO cells in the utility insertion. For the best configuration we have then tracked the particles, with $\delta$=0 and $\delta \neq 0$, to obtain the dynamics apertures. These have been finally obtained using a faster tracking code, RACETRACK.

The performances of an improved case, from the point of view of dynamic aperture are also included in table 1 ($3^{rd}$ column). In this case we have two additional sextupoles families in the utility insertion, where we have made $D_x \neq 0$, to help the correction of chromaticities.

In all cases the rings were considered to be perfect, without any closed orbit or field errors. However the synchrotron radiation damping has not been included.

| | TBA M-LE | TBA S-HE | TBA S-HE ($D_x \neq 0$) | |
|---|---|---|---|---|
| $E_0$ | 2.0 | 2.0 | 2.0 | GeV |
| $\rho$ | 6.31 | 6.31 | 6.31 | m |
| $\sigma_\epsilon$ | $6.81\ 10^{-4}$ | $6.81\ 10^{-4}$ | $6.81\ 10^{-4}$ | |
| C | 387.0 | 387.0 | 387.0 | m |
| $k_b f_r$ | 27.89 | 27.89 | 27.87 | MHz |
| $\kappa$ | 0.067 | 0.033 | 0.033 | |
| $\epsilon_x$ | $1.9\ 10^{-8}$ | $2.9\ 10^{-7}$ | $2.7\ 10^{-7}$ | m rad |
| $\epsilon_y$ | $1.3\ 10^{-9}$ | $9.5\ 10^{-9}$ | $9.1\ 10^{-9}$ | m rad |
| $\beta_x^*$ | 0.01 | 0.3 | 0.3 | m |
| $\beta_y^*$ | 0.15 | 0.01 | 0.01 | m |
| $D_y^*$ | 0.32 | 0.0 | 0.0 | m |
| $\xi_x$ | 0.04 | 0.04 | 0.04 | |
| $\xi_y$ | 0.035 | 0.04 | 0.04 | |
| $N_b$ | $1.2\ 10^{11}$ | $1.1\ 10^{11}$ | $1.0\ 10^{11}$ | |
| I | 0.55 | 0.47 | 0.50 | A |
| L | $1.1\ 10^{33}$ | $8.4\ 10^{32}$ | $8.0\ 10^{32}$ | $cm^{-2}s^{-1}$ |
| $\lambda$ | 15.8 | 1.0 | 1.0 | |
| $\sigma_w$ | 0.1 | 1.9 | 1.9 | MeV |
| $Q_x$ | 18.4 | 11.5 | 10.9 | |
| $Q_y$ | 10.7 | 15.1 | 14.5 | |
| $Q'_x$ | -40.9 | -32.6 | -31.8 | |
| $Q'_y$ | - 41.9 | -40.4 | -39.8 | |
| $SF$ | 53.3 | 41.0 | 37.9 | T/m |
| $SD$ | -80.3 | -46.7 | -44.5 | T/m |
| $A_x$ | 30 | 12 | 21 | $\sigma^*_{x\beta}$ |
| $A_y$ | 84 | 68 | 67 | $\sigma^*_{y\beta}$ |
| $V_{RF}$ | 2.0 | 12.0 | 12.0 | MV |
| $h$ | 612 | 612 | 612 | |
| $\sigma_b$ | $5.8\ 10^{-3}$ | $6.0\ 10^{-3}$ | $6.1\ 10^{-3}$ | m |
| $\epsilon_{RF}$ | 0.024 | 0.024 | 0.023 | |
| $\epsilon_E$ | 0.018 | 0.022 | 0.021 | |
| $\tau_{tr}$ | 166.0 | 4813.6 | 4679.7 | min |
| $\tau_{bb}$ | 400.5 | 410.4 | 404.2 | min |

Table 1: Performances of the TBA lattice in the two modes of operation.

## 3 BEAM LIFETIME

In a TCF the two main contributions to the lifetime are the Touschek effect and the beam-beam bremsstrahlung.

The Touschek effect is important at low and medium energies, with flat beams and low emittance. Hence in the monochromatic case the beam lifetime comes essentially from this effect.

To compute the Touschek lifetime, $\tau_{tr}$ [9] it is necessary to know the energy acceptance of the machine, $\epsilon_E$. Both

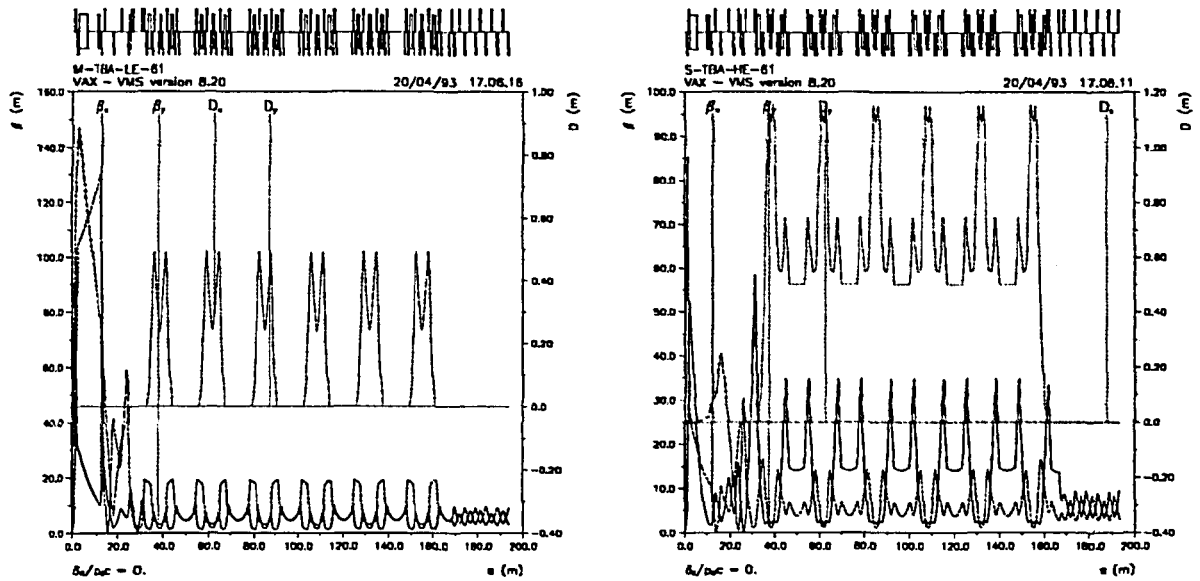

(a) Monochromatization. (b) Standard.

Figure 1: Optics along one superperiod of the TBA lattice.

energy acceptance and Touschek lifetime have been calculated using a numerical code [10] which takes into account the jumps in particle energy from this effect all around the ring.

In a very high luminosity machine the beam lifetime may also come from beam-beam inelastic collisions ($e^+e^-$ bremsstrahlung). The lifetime due to this effect, $\tau_{bb}$, has been calculated with the usual formula [11]. The energy acceptance at IP, $\epsilon_E^*$, is calculated with the code [10], and found to be equal to the RF acceptance, $\epsilon_{RF}$. The results are summarized in table 1.

## 4 CONCLUSION

From this feasibility study we can conclude that a single ring geometry can include both monochromatization and standard schemes with the same luminosity, 1.0 $10^{33}$ cm$^{-2}$ s$^{-1}$ at $E_0$ =2.0 GeV.

Concerning the arcs, we have observed that TBA cells, although non-conventional for a collider, are more flexible than FODO arcs. Hence we can change from low (2.0 $10^{-8}$ m rad) to high (3.0 $10^{-7}$ m rad) emittance by simple detuning of the optics without additional quadrupoles in the arcs and without wigglers.

The beam lifetimes have been considered also. In the standard mode beam-beam bremsstrahlung is the dominant loss mechanism. However in the monochromatic mode the high beam density causes the Touschek effect to dominate.

## 5 REFERENCES


[1] J. Gonichon, J. Le Duff, B. Mouton and C. Travier "Preliminary study of a high luminosity $e^+e^-$ storage ring at a CM energy of 5 Gev" (LAL-RT 90-02, January 1990)

[2] J.M. Jowett "Feasibility of a monochromator scheme in LEP" (CERN LEP Note 544, September 1985)

[3] A. Faus-Golfe and J. Le Duff "A versatile lattice for a Tau-Charm factory that includes a monochromatization scheme" (LAL-RT 92-01, February 1992)

[4] A.A. Zholents "An electron-positron factory for polarized J/Ψ mesons" (CERN SL/92-27 (AP), June 1992)

[5] A.L. Gerasimov, D.N. Shatilov and A.A. Zholents "Beam-Beam effects with large dispersion function at the interaction point" (Nuclear Instruments and Methods in Physics Research A305 (1991) 25-29)

[6] P.F. Beloshitsky "A magnet lattice for a Tau-Charm factory suitable for both standard scheme and monochromatization scheme" (LAL-RT/92-09, July 1992)

[7] A. Faus-Golfe and J. Le Duff " A Versatile Lattice for a Tau-Charm factory that includes a Monochromatization Scheme (Low-Emittance) and a Standard Scheme (High-Emittance)" (Proc. of IEEE Particle Accelerator Conference, 1993 Washington)

[8] A. Faus-Golfe "Etude d'un anneau $e^+e^-$ à très haute luminosité, avec et sans monochromatization des faisceaux (cas particulier d'une usine Tau-Charme)" (Thèse de doctorat LAL 94-02, Janvier 1994)

[9] R.P. Walker "Calculation of the Touschek lifetime in $e^+e^-$ storage rings" (Proc. of IEEE Particle Accelerator Conference Vol.1 pag. 491, 1987 Washington)

[10] Y. Alexahin "Calculation of the Touschek lifetime (relativistic)" (JINR Dubna, communication privée)

[11] J. Haissinski "Bremsstrahlung simple dans les collisions negatons-positons" (RT-5-64 Anneaux de stockage, Laboratoire de l'Accélérateur Linéaire, Orsay 1964)